Anti-infective DNase I Coatings on Polydopamine Functionalized Titanium Surfaces by Alternating Current Electrophoretic Deposition

M. K. Aktan[a,†], M. Van der Gucht[b,†], H. Hendrix[b], G. Vande Velde[c], K. Baert[d], T. Hauffman[d], M. S. Killian[e,f], R. Lavigne[b,*], A. Braem[a,*]

[a]KU Leuven, Department of Materials Engineering (MTM), Biomaterials and Tissue Engineering Research Group, Kasteelpark Arenberg 44 - box 2450, 3001 Leuven, Belgium

[b] KU Leuven, Department of Biosystems, Laboratory of Gene Technology, Kasteelpark Arenberg 21 - box 2462, 3001 Leuven, Belgium

[c] KU Leuven, Department of Imaging & Pathology, Biomedical MRI/ MoSAIC, Herestraat 49 - box 7003, 3000 Leuven, Belgium

[d]Research Group of Electrochemical and Surface Engineering (SURF), Department of Materials and Chemistry (MACH), Vrije Universiteit Brussel, Pleinlaan 2, Brussels, Belgium

[e]Chemistry and Structure of Novel Materials, University of Siegen, Paul-Bonatz-Str. 9-11, Siegen 57076, Germany

[†]These authors contributed equally

*Correspondence: Prof. Annabel Braem (e-mail: annabel.braem@kuleuven.be; Tel: +32 16 32 15 34) and Prof. Rob Lavigne (e-mail: rob.lavigne@kuleuven.be; Tel: +32 16 37 95 24)

Abstract

Implant-associated infections (IAIs) can cause serious problems due to the difficult-to-treat nature of biofilms formed on the implant surface. The biofilm matrix, consisting of polysaccharides, proteins, lipids and extracellular DNA (eDNA), forms a protective environment for the residing bacteria in mature biofilms. Recently, indirect prevention of biofilm growth through the degradation of eDNA using an enzyme, such as deoxyribonuclease (DNase) I, is being considered a promising strategy in the battle against IAIs. In this study, the immobilization of protective DNase I coatings on titanium implant materials was investigated. The effectiveness of alternating current electrophoretic deposition (AC-EPD) as a novel processing route to apply DNase I on titanium using polydopamine (PDA) as an intermediate was examined and compared with the commonly applied diffusion methodology (i.e. classic dipping). The use of AC-EPD significantly increased the amount of deposited protein for the same processing time, yielding homogeneous coatings with a thickness of 12.8 nm and increased average surface roughness, S_a, of ~20

nm. The surface free energy components revealed an increase in γ^- from 10.2 to ~20 mJ m^{-2} upon PDA functionalization and enzyme coating regardless of the coating procedure, indicating monopolar surfaces with increased electron-donor capacity . Furthermore, X-ray photoelectron spectroscopy confirmed the presence of peptide bonds on all DNase-coated substrates. Time-of-flight secondary ion mass spectrometry detected a more dense DNase I layer in the case of AC-EPD, which was selectively deposited on the electrode coupled as anode during the high-amplitude half cycle of AC signal. Disulfide signals did not differ from those obtained from a dipped DNase reference sample, confirming that the tertiary enzyme structure was not influenced by the deposition methodology. The enzyme activity, release kinetics, and shelf life of DNase I coatings were monitored in real-time using a quantitative qDNase assay. DNase I coatings produced using AC-EPD are threefold more active compared to coatings prepared by classic dipping. In line with covalent linking of DNase to PDA, both deposition methods enable a stable attachment of a small fraction of the DNase activity to the surface, while loosely adhering superimposing DNase deposits are released from the surface in a high burst. Interestingly, coatings prepared with AC-EPD exhibit a prolonged, gradual release of DNase activity. The AC-EPD DNase coatings significantly reduce biofilm formation of both *Staphylococcus epidermidis* and *Pseudomonas aeruginosa* up to 20 h, whereas DNase coatings prepared by short classic dipping only reduce *S. epidermidis* biofilm formation, and to a lesser extent. Overall, this study indicates that AC-EPD allows to rapidly concentrate DNase I on PDA-functionalized titanium, while maintaining the enzyme activity and anti-infectivity properties. This highlights the potential of AC-EPD as a time-efficient coating strategy (as opposed to the much slower dip-coating methodologies) for bioactive molecules in a wide variety of biomedical applications.

Keywords

Implant-associated Infections; Surface modification; Polydopamine; Alternating current electrophoretic deposition; DNase I; Biofilm prevention;

Abbreviations

AC-EPD: alternating current electrophoretic deposition, DNase I: deoxyribonuclease I, PJI: prosthetic joint infections, Ti: titanium, eDNA: extracellular DNA, DA: dopamine, PDA: polydopamine, pol-Ti: polished titanium, pDA-Ti: polydopamine functionalized-titanium, DNase-EPD: DNase-coated titanium by AC-EPD, DNase-dip: DNase-coated titanium by classic dipping

1. Introduction

While the need for medical implants continues to grow, infection remains one of the major causes of implant failure [1]. For internal implants such as prosthetic joints, the infection incidence is fairly low, about 1% for hip and knee implants and up to 5% for elbow replacements. By contrast, in percutaneous devices the incidence can increase up to 26.6% for urinary catheters and even 38.6% for cardiac implantable devices [2,3]. Although prosthetic joint infections (PJIs) appear less problematic in absolute numbers, they are extremely difficult to treat and consequently one of the leading causes of implant failure [4,5]. Furthermore, PJIs are associated to an increased number of complications, length of hospitalization and hospital readmission, all of which reduce the patient's quality of life and raise healthcare expenses [6–9]. Moreover, PJIs are associated with mortality rates around 2.7 – 18% in the US [10]. Alarmingly, increased infection rates have been observed in recent years. For example, the Swedish Hip Arthroplasty Register noted an increased incidence of infections from 0.7 to 1.3% between 1999 and 2019 [11]. This is expected to continue in the coming years due to the rising demand for joint replacements combined with an increase in patients with infection risk factors such as rheumatoid arthritis and obesity [12–14]. Over the years, titanium (Ti) and its alloys have found widespread use in orthopedic applications due to their excellent mechanical and physiological performance [15]. However, Ti is biologically inert and as such does not promote antimicrobial activity.

The most common bacterial species isolated from PJIs are Gram-positive *Staphylococcus aureus* (*S. aureus*) in the USA and *Staphylococcus epidermidis* (*S. epidermidis*) in Europe, together representing more than 60% of infections. The most common Gram-negative species is *Pseudomonas aeruginosa* (*P. aeruginosa*) [16–18]. Although representing a smaller fraction of approximately 6% of the PJIs, treatment of *P. aeruginosa* infections are considered to be one of the most challenging due to the common incidence of multidrug resistance and its extreme virulence and persistence [19].

It is generally accepted that bacteria involved in implant-associated infections exist in biofilms [20]. These are structured, surface-adhering bacterial communities embedded in a biofilm matrix [21]. This matrix is composed of self-produced extracellular polymeric substances (EPS), including polysaccharides, proteins, lipids and extracellular DNA (eDNA), and plays a pivotal role by holding the bacteria together and attaching them to the surface [22,23]. Remarkably, the biofilm lifestyle protects the residing bacteria from the attacks by the immune system and antibiotics, making mature biofilms up to 100-1,000 fold less susceptible to antibiotic treatments [24,25]. Alarmingly, all materials currently used in prosthetics, including Ti, stainless steel, cobalt-chromium, PMMA and various polymeric biomaterials, are prone to bacterial attachment and biofilm development [26–28].

The difficult-to-treat nature of biofilms encourages researchers to develop strategies to prevent the formation of implant-associated biofilms, rather than eradicate established biofilms. In this regard, extracellular DNA (eDNA) is an excellent target. eDNA plays an active role in the formation of biofilms, contributing to surface attachment and cell-to-cell adhesion [29]. Interestingly, degradation of eDNA by DNA-degrading enzymes, called deoxyribonucleases (DNases), can inhibit biofilm formation of multiple bacterial species, including *S. aureus*, *S. epidermidis* and *P. aeruginosa* [30,31]. This indicates that eDNA is a common target among the implant infection-related bacteria and that DNases are broad-spectrum anti-infective agents. DNases can be generally considered safe to be used in human applications. For example, a formulation of human recombinant DNase I commercialized by Roche (Basel, Switzerland), has been FDA-approved to improve the lung functioning of Cystic Fibrosis patients [32,33].

In this work, we aim to develop an efficient strategy to prevent implant-associated infections by immobilizing bovine DNase I on Ti implant surfaces, pursuing the presence of active DNases at the potential infection site. Previous work by Swartjes *et al.* (2013), Yuan *et al*. (2014), Alves *et al.* (2016) and Ye *et al.* (2017) indicated that DNase I can be coupled to various substrates (i.e. poly-dimethylsiloxane, poly(styrene-b-isobutylene-b-styrene), polymethylmethacrylate and Ti), creating coatings that effectively inhibit biofilm formation *in vitro* [34–37]. The common strategy includes activating the surface with coupling agents (i.e. polycarboxylates or PDA), followed by DNase deposition from a suspension by classic dipping. Nonetheless, this coating by dipping relies on long dipping times (several hours up to days) due to slow passive diffusion of biomolecules towards the implant surface. Besides long processing times, this most likely implies loss of enzyme activity by protein destabilization and degradation over time. An alternative DNase coating strategy using a poly-(lactic-co-glycolic)-acid (PLGA) overcoat enabled gradual DNase release from the surface, which was also effectively reducing biofilm formation [38].

Here, we propose electrophoretic deposition (EPD) as a rapid and efficient alternative to prepare homogeneous and active DNase I coatings on Ti. This colloidal technique uses the electrophoretic movement of charged particles in a suspension under an applied electric field to obtain deposition on the electrode surface in an orderly manner [39]. In this way, coatings could be applied on a wide range of materials and substrate shapes in a cost-effective way. EPD of inorganic particles is usually carried out by application of direct current (DC) fields. However, the use of DC fields in an aqueous medium causes water electrolysis when the applied voltage exceeds 1.23 V at 25°C, resulting in pH shifts and Joule heating [40]. Interestingly, the use of asymmetric alternating current (AC) electric fields reduces water electrolysis while ensuring a net migration of the particles in suspension, and is therefore preferred for the deposition of molecules from aqueous suspensions [40–44]. AC-EPD has already been applied successfully to deposit

antifungals, enzymes and even bacterial cells within a short processing time, while maintaining the intrinsic functionalities [45–47]. To introduce sufficient functional groups on the surface of Ti, dopamine (DA) which consists of catechol and amine (-NH_2) functional groups, was chosen to enable covalent grafting of biomolecules on the Ti substrate. At alkaline pH, DA undergoes a self-polymerization reaction and forms polydopamine (PDA) on a wide variety of substrates, including metals. This PDA layer will work as a mediator between the metal surface and a DNase I top coating.

In this study, we aim to establish a proof-of-concept for the fast immobilization of DNase I on PDA-functionalized Ti surfaces via AC-EPD. DNase I coatings were prepared for 10 min by both AC-EPD and classic dipping, and a comparative study was carried out with a variety of characterization techniques to evaluate the performance for the intended application as anti-infective coatings. First, the sample substrates were characterized after various processing steps in terms of surface morphology via scanning electron microscopy (SEM) and atomic force microscopy (AFM); coating thickness via ellipsometry; and wettability and surface free energy via contact angle measurements. Furthermore, surface chemistry evaluation was carried out via X-ray photoelectron spectroscopy (XPS) and time-of-flight secondary ion mass spectrometry (ToF-SIMS). Next, the activity, shelf life and release kinetics of DNase coated samples were assessed using a qDNase assay. Finally, the DNase coatings were evaluated for their ability to reduce biofilm formation *in vitro* of two relevant implant-associated pathogens, *S. epidermidis* and *P. aeruginosa,* by SEM and confocal laser scanning microscopy (CLSM).

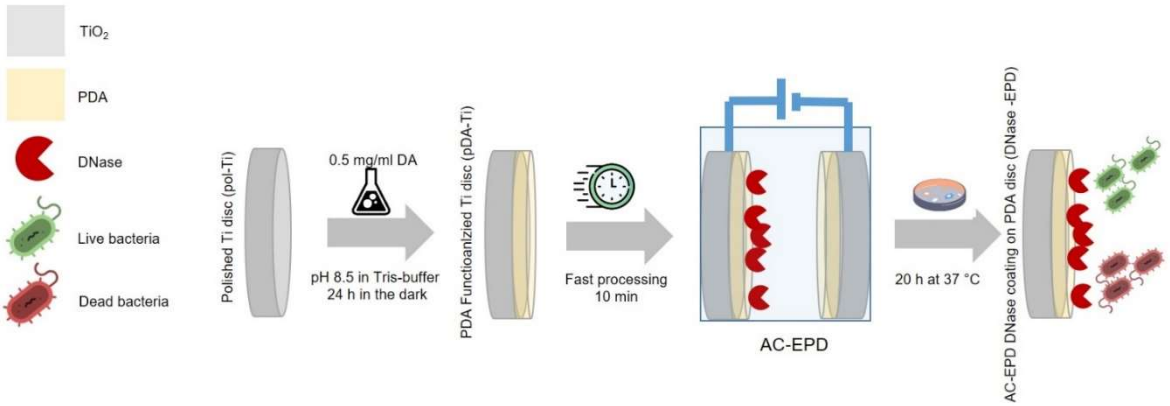

Figure 1. Schematic representation of the antibacterial coating methodology. Polished Ti discs (pol-Ti) are functionalized using a 0.5 mg mL-1 dopamine starting concentration, resulting in a functional intermediate layer on Ti (pDA-Ti). Next, PDA-functionalized Ti discs serve as electrode during the alternating current electrophoretic deposition (AC-EPD) of DNases resulting in the formation of a DNase

coating after 10 min of the deposition process (DNase-EPD). Lastly, in vitro anti-infective activity of DNase-coated Ti substrates against 20 h-old Staphylococcus epidermidis and Pseudomonas aeruginosa biofilms was evaluated.

2. Materials and Methods

2.1. Substrate preparation. Ti discs (grade 2, Ø=5mm, thickness=2mm; Salomon's Metalen, the Netherlands) were ground with an automatic polishing machine (Struers, Denmark) equipped with resin bonded diamond grinding discs (MD-Mezzo 220 and MD Largo; Struers) followed by polishing with an Oxide Polishing Suspension (OPS; colloidal silica, Microdiamant, Germany) and hydrogen peroxide (H_2O_2; 35 wt%, Chem-Lab, Belgium) mixture (70:30 by vol%) on a synthetic polishing cloth (Galaxy Polishing Cloth Omega; Advanced Metallography, Germany). All samples were cleaned with acetone (>99%, Chem-Lab) for 20 min in an ultrasonic bath (model 2510, Branson) followed by extensive rinsing with ultra-pure water (milliQ, 18.2 µs cm^{-1}, Merck Millipore, USA) and technical ethanol (Disolol, Chem-Lab). These pristine polished Ti substrates (pol-Ti) were further functionalized with a PDA layer by immersing them for 24 h in a 0.5 mg mL^{-1} dopamine (DA, 99%; Alfa Aesar, USA) solution in Tris buffer (10 mM, pH 8.5; Acros Organics, Belgium) at 22°C in an incubator (MIR-154, Cooled Incubator; Panasonic, Japan) in the dark. The samples were ultrasonically cleaned (model 2510, Branson, USA) with milliQ for 5 min. The resulting PDA-functionalized Ti substrates (pDA-Ti) were dried in an incubator (MIR-154 Cooled Incubator, Panasonic, Japan) and stored at 4°C until further use.

2.2. DNase I suspension preparation and characterization. Aqueous suspensions of 0.0125 mg mL^{-1} deoxyribonuclease I from bovine pancreas Type IV (DNase I, 2814 U mg^{-1}, D5025; Sigma-Aldrich, USA) were prepared fresh in milliQ by gentle pipetting before every experiments. The conductivity and pH of the suspensions was measured by a micro conductivity probe (InLab 751-4 mm; Mettler Toledo, USA) and a micro pH electrode (InLab Micro; Mettler Toledo), respectively. The zeta potential of DNase I was determined by electrophoretic light scattering (Zetasizer Nano ZS, Malvern Instruments, UK) in the fast field reversal mode in order to prevent denaturation of the enzyme by Joule heating. To estimate the isoelectric point (IEP) of DNase I, the zeta potential was monitored as function of pH by stepwise decreasing or increasing the suspension pH by adding 0.05 M HCl (37%, VWR, Germany) or 0.05 M NaOH (32%, VWR), respectively. For coating procedures by long-term (~6 h) immersion, the 0.0125 mg mL^{-1} DNase I suspension was prepared in phosphate buffer (4.6 mM K_2HPO_4, 5.4 mM KH_2PO_4, 150 mM NaCl, 10 mM $MgCl_2$, pH 6.8), as reported previously [34,37].

2.3. Alternating current electrophoretic deposition versus classic dipping. AC-EPD was carried out in the controlled-current mode under ambient conditions. A schematic representation of the deposition cell is given in **Figure 1.** Custom-made Ti clips (**Figure S1**) were placed around the pDA-Ti discs to ensure electrical contact along the side of the discs and two identical electrode systems were inserted in polystyrene cuvettes (Macrocuvette, VWR). The electrodes were separated at a fixed distance of 0.8 cm using a polytetrafluorethylene spacer. As in our earlier work, an asymmetrical triangular AC signal with an asymmetry of 3 and a frequency of 100 Hz was generated using a high-resolution digital-to-analog signal output module (NI9269, National Instruments, Belgium) and amplified with a bipolar amplifier (PZD 7000 M S^{-1}, Trek Inc, USA) [47]. A peak-to-peak current of 6 mA cm^{-2} was applied for 10 min. Current and voltage were monitored by an analog-to-digital acquisition module (NI9223, National Instruments) linked to the monitor channels of the operational amplifier. Afterwards, the substrates were removed from the cuvette and rinsed by gently dipping in milliQ water followed by drying at room temperature. The resulting DNase-EPD electrodes, i.e. DNase-EPD anode and DNase-EPD cathode, were stored at 4°C until further use. For simplicity, samples further denominated as DNase-EPD refer to DNase-EPD anode, unless otherwise specified. For comparison, a classic dipping experiment was conducted for 10 min using the same DNase I suspension as well as the same deposition cell. Samples, denominated as DNase-dip, were rinsed and dried in the same way as the DNase-EPD samples.

2.4. Coating characterization. *2.4.1. Scanning electron microscope (SEM).* Surface features of the various samples were visualized using SEM (Nova NanoSEM 450, FEI, USA) with an in-lens secondary electron detector (magnetic immersion lens) for a higher nano-scale resolution. The SEM was operated at a working distance of 5 mm and a low accelerating voltage of 5 keV to increase the surface sensitivity of the imaging and to minimize beam damage on the enzyme coatings. Prior to SEM, a thin (~2 nm) Pt layer was sputter-coated (Q150T ES plus, Quorum, UK) on the surface to improve the conductivity.

2.4.2 *Atomic force microscopy (AFM).* High-resolution topography images were obtained by AFM operated in the non-contact mode (PicoSPM 5500, Agilent Technologies, USA) using a silicon cantilever (AC160TS-R3, Olympus, Japan) in ambient conditions. An area of 6 x 6 μm^2 (1024 x 1024 pixels) was scanned for each sample. The arithmetic mean height of a surface (S_a) profile was calculated using the WSXM software (version 5.0, Nanotec, Spain) [48].

2.4.3. Spectroscopic ellipsometry. The thickness and refractive index of various DNase coatings were measured via spectroscopic ellipsometry (iSE Ellipsometer, J.A. Woollam, USA) in the wavelength range between 400-1000 nm at a 70° incidence angle. Modelling of the ellipsometry data was done using the Complete EASE operating software (version 5.2, J. A. Woollam). A multi-layer optical model was used to

analyze the coating thickness, which comprises of a B-spline model for the native TiO_2 layer on the pol-Ti substrates, a Cauchy model for the PDA layer of pDA-Ti and a Cauchy model for DNase I coatings. Based on measurement, the native TiO_2 layer and the PDA layer, the film thickness (d_f) and the refractive index of the film (n_f) were fixed as d_{TiO2} of 4.4 nm, d_{PDA} of 16.9 and n_{TiO2} of 2.17, n_{PDA} of 1.48, respectively. For DNase I coatings, the reported values for thickness and refractive index are an average of three replicates. To quantify the amount of adsorbed DNase I (ng mm^{-2}) on pDA-Ti, the d_f and n_f of each DNase I film was used in the de Feijter formula (Eq. 2) [49]. The refractive index value of ambient air (n_m: 1) was considered for the calculation and 0.18 $cm^3\ g^{-1}$ was used as the protein refractive index increment ($^{d_n}/_{d_c}$)[50].

$$\Gamma\ (\text{ng mm}^{-2}) = \frac{d_f(n_f - n_m)}{{}^{d_n}/_{d_c}} \quad \text{Eq. 1}$$

2.4.4. Contact angle measurements. The surface wettability and surface free energy (SFE) were analyzed using an Optical Contact Angle and Contour Analysis System (OCA 15EC, Dataphysics, Germany) applying the sessile drop method for static contact angle measurement. To calculate the contact angles of each measurement liquid (i.e., one dispersive liquid (diiodomethane, 99%, Acros Organics) and two polar liquids (milliQ water and ethylene glycol, 99.5%, Acros Organics, respectively)), the video contact angle system using a software-operated fitting procedure (SCA 20 software, Dataphysics) was employed[51].

According to the van Oss, Chaudhury and Good (vOCG) equation 2, the SFE components, i.e., the non-polar component (the dispersive Lifshitz-van der Waal; γ_s^{LW}) and polar components (acid; γ_s^+, base; γ_s^-)) were calculated using the SCA 20 software (Dataphysics) [52].

$$\sqrt{\gamma_s^{LW}\gamma_l^{LW}} + \sqrt{\gamma_s^+\gamma_l^-} + \sqrt{\gamma_s^-\gamma_l^+} = 0.5\,\Upsilon_{lv}\,(1 + \cos\theta) \quad \text{Eq. 2}$$

The polar component, γ^{AB}, and total surface free energy, γ^{tot}, were determined using following equations Eq. 3 and Eq. 4 [53]. Reported values are an average of five replicate samples.

$$\gamma^{AB} = 2\sqrt{\gamma^+\gamma^-} \quad \text{Eq. 3}$$

$$\gamma^{tot} = \gamma^{LW} + \gamma^{AB} \quad \text{Eq. 4}$$

2.4.5. Scanning X-ray Photoelectron Spectroscopy (XPS) microprobe analysis. The surface chemistry was characterized by XPS (PHI VersaProbe III, Physical Electronics, USA) using $Al_{K\alpha}$ monochromated radiation (1486.6 eV; 24.9 W) as the exciting source and a pressure of 10^{-7} Pa. High-resolution spectra of the target elements (Ti 2p, O 1s, C 1s, N 1s) were recorded with a pass energy of 26 eV, a step size of 0.05 eV and a spot size of 100 µm. The calculated composition (in at%) was based on internal sensitivity factors in Multipak (Multipak, PHI software). Before curve fitting, the binding energy scale was calibrated by the C

1s peak at 284.7 eV. C 1s, N 1s and O 1s core level spectra were deconvoluted via CasaXPS software and a Shirley-type background correction was used along with mixed Gaussian-Lorentzian shapes with a typical ratio of 70:30. Detailed information on the peak fitting is summarized in the Materials and Methods section of the Supporting Information.

2.4.6. Time-of-Flight Secondary Ion Mass Spectrometry (ToF-SIMS). To evaluate the surface chemistry of the Ti substrates after several surface treatments, positive and negative static SIMS measurements were recorded on a ToF-SIMS spectrometer (ToF.SIMS 4, ION-TOF, Germany). Spectra were recorded in the high mass resolution mode using a pulsed 25 keV Bi^{3+} liquid-metal ion beam in static conditions (primary ion dose density = 5 x 10^{11} ions cm^{-2}). Poisson corrected spectra were calibrated to CH_3^+, $C_2H_3^+$, $C_3H_5^+$, $C_4H_9^+$ and $C_7H_7^+$ (C^-, CH-, CH_2^- and C_2^- for negative polarity, respectively). Spectra showing artefacts from ion beam instabilities (e.g., peak broadening, low total spectral intensity) were omitted from analysis. The "spectragui" software from the NESAC/BIO toolbox was applied for principal component analysis (PCA) [54]. The peak set used for PCA processing of the positive spectra is described in the Supporting Information, **Table S1**. A peak list containing amino acid (AA), PDA and substrate fragments was compiled according to literature [55]. Fragments that were too close to produce clearly distinguishable signals were combined. The PDA and substrate fragments were identified by comparing PDA to DNAse or Ti samples via PCA. The total intensity of the PCA peak set was used for spectra normalization and square root mean-centering was used to ensure the differences in samples are caused by variations around the means and not the variance of the means [56].

2.5. Enzymatic assays. *2.5.1. DNase activity assays.* DNase activity of discs or suspensions was measured using the qDNase assay as described previously [57]. In short, discs or suspensions were placed in a black polystyrene 96-well plate (Nunc™, Thermo Scientific, USA) to which the reaction mixture was added to a final concentration of 200 nM DNaseAlert™ substrate, 1x DNaseAlert™ buffer (IDT, USA) and 150 mM NaCl (Acros Organics) in 100 µl. At regular time intervals, the fluorescent signal was measured (excitation: 520 nm / emission: 570 nm) on a CLARIOStar plus multimode microplate reader (BMG LABTECH, Germany) at 37°C with 5 s double orbital shaking (300 rpm) between readings. The relative activity (in RFU s^{-1}) was calculated from a negative control-corrected fluorescence curve as the slope of the initial linear region corresponding to the dataset with maximized R^2-value. Described activities are always represented as average ± standard deviation from the parallel analysis of at least three replicate DNase-coatings or suspensions. To convert relative activities to absolute units of DNase I, calibration curves were made by measuring the activity of different DNase I concentrations under the exact same reaction conditions and set-up as described above. For specific activity assays (i.e. surface activity after 6 h immersion, released

activity in Phosphate Buffered Saline (PBS, 137 mM NaCl, 2.7 mM KCl, 10 mM Na_2HPO_4, 1.8 mM KH_2PO_4) and remaining surface activity after the release experiment), NaCl was left out of the reaction mixture to increase the sensitivity of the assay. In this case, calibration curves were generated by measuring the activity of different DNase I concentrations in the absence of NaCl.

2.5.2. Coating stability. Discs were stored dry at 4°C. After 1, 3 and 7 days, their activity was measured and compared relatively to the activity of fresh corresponding fresh DNase coatings.

2.5.3. Release of DNase I from surface. To analyze the release profile of DNase coatings, discs were immersed in 200 µl PBS at 4°C under gentle shaking (@ 20 rpm). At 0, 0.5, 1, 2, 4, and 24 h, 10 µl samples were taken from the PBS, replaced with 10 µl precooled PBS (4°C) and assessed for DNase activity. After 24 h, discs were rinsed with milliQ, dried and assessed for activity.

2.6. Biofilm assays. *2.6.1. Biofilm growth on Ti discs.* A single colony of *P. aeruginosa* strain PAO1 (ATCC 15692) or *S. epidermidis* strain DH3LIK [58] was used to inoculate Lysogeny Broth (LB; 10 g L^{-1} Tryptone, 5 g L^{-1} Yeast Extract, 10 g L^{-1} NaCl) or Tryptone Soya Broth (TSB), respectively. The cultures were grown overnight at 37°C. The next day, these overnight cultures were washed three times in PBS, 1:100 diluted in LB (PAO1) or TSB + 0.25% glucose (DH3LIK) and supplemented with 10 mM $MgCl_2$ and 1 mM $CaCl_2$. Discs were inserted in 24-well plates and covered with 1.2 ml inoculum. Biofilms were grown for 20 h at 37°C under static conditions.

2.6.2. Biofilm observation by SEM. Biofilms were gently rinsed in PBS and fixed for 30 min using 2.5% glutaraldehyde (glutaraldehyde grade I, 25%, Sigma-Aldrich) in 0.1 M cacodylate buffer (pH 7.4). Next, biofilms were washed three times with PBS and dehydrated with an ethanol gradient by immersing the biofilms consecutively in 30%, 50%, 70%, 90% and three times 100% ethanol for 20 min. The fixed biofilms were observed by SEM. The SEM was operated under high-vacuum settings using a high-resolution in-lens SE detector (magnetic immersion lens) or BSE. A low accelerating voltage (3 keV) was used together with a stage-bias of 1-2 keV to minimize beam damage on the biofilm matrix. The working distance and spot size were set to 5 mm and 3, respectively. Prior to SEM imaging, a sputtering device (Edwards S150, UK) was used to generate an Au conductive layer on the samples.

2.6.3. Biofilm quantification by Confocal Laser Scanning Microscopy (*CLSM).* Biofilm formation was quantified by CLSM analysis. The biofilms were washed in saline (0.85% NaCl) and stained using the LIVE/DEAD® BacLight™ Bacterial viability kit (L7012, Invitrogen, USA) according to the manufacturer's instructions. Next, discs were placed on a glass bottom dish (Cellvis, USA). Biofilms were faced down and immersed in a minimal volume of milliQ to prevent dehydration of the samples. Visualization was performed on an inverted Leica true confocal scanner SP8 X system (Wetzlar, Germany) equipped with a

HC PL APO 10x dry objective (NA 0.4) using the green and red fluorescence channel. For each sample, z-stacks were acquired on three different positions with an image size of 1024 x 1024 pixel^2, a pixel size of 1.14 × 1.14 µm^2 and a z-step size of 2.00 µm. CLSM images represent the sum of all slices in the corresponding stack and were composed using Fiji [59,60]. For each stack, biofilm parameters were calculated with Comstat2 using Automatic Treshold (Otsu's Method) and Connected Volume Filtering [61–63]. The biovolume was calculated as the sum of the biovolume of live (green) and dead (red) bacteria, whereas all other biofilm parameters were retrieved from live (green) bacteria only. Data visualizations were made with GraphPad Prism 8.4.3.

2.7. Statistical analysis. An initial Kolmogorov-Smirnov normality test was performed using GraphPad Prism version 9.0.2 for Windows to determine whether a given dataset was normally distributed. Subsequently, a *t*-test (parametric) or Mann-Whitney test (non-parametric) was performed to compare the effect of two different coatings on a specific biofilm parameter.

3. Results

To evaluate AC-EPD as an alternative for classic dipping to prepare anti-infective DNase I coatings on PDA-functionalized Ti substrates (pDA-Ti), both methods were compared. First, key morphological and chemical properties of the coated surfaces after various processing steps were determined. Next, the enzymatic activity and its release from the surface over time were compared, followed by an *in vitro* evaluation of the efficacy of the DNase I coatings to prevent biofilm formation.

3.1. AC-EPD improves the deposition yield of DNase I on PDA-functionalized titanium surfaces

To assess the suspension stability as well as the migration direction and velocity of the particles during EPD, the zeta potential of the DNase I suspension was determined as function of pH (**Figure S2**). From the pH titration curve, the IEP of the enzyme could be determined at a pH of 5.2 [64]. At the natural pH of the suspension (i.e. ~6.5), DNase I exhibited a zeta potential of -22 mV. Furthermore, based on the negative sign of the zeta potential, it could be expected that DNase I will preferentially deposit on the electrode coupled as anode during the high-amplitude half cycle during AC-EPD. The conductivity of the DNase suspension was measured to be 61.8 µS cm^{-1}.

Next, DNase I coatings were prepared by AC-EPD as indicated above and are hereafter referred to as DNase-EPD (**Figure 1**). PDA-functionalized Ti substrates were applied, as this coupling layer has been shown to improve the long-term immobilization of proteins on a wide variety of substrates, including metals [65,66]. Initial experiments showed that AC signals above 150 V cm^{-1} resulted in Joule heating and

bubble formation at the electrode surface. Therefore, AC signals were kept below 150 V cm^{-1} to prevent denaturation and concomitant loss of activity of the enzyme. The peak-to-peak amplitude of the AC field was optimized via a trial-and-error approach by measuring the deposited enzyme activity with the qDNase assay. Using a frequency of 100 Hz, a peak-to-peak current, I_{p-p}, of 6 mA cm^{-2} (corresponding to approximately 3 mA or 120 V cm^{-1}) resulted in an optimal activity with the highest repeatability (**Figure S3a**). Both electrodes (i.e. the anode and cathode during the high-amplitude half cycle) were tested using the qDNase assay. The relative activity of the electrodes is shown in **Figure S3b**. The activity detected at the anode was significantly higher compared to the cathode. Therefore, all further analyses on DNase-EPD samples were performed on the electrode serving as the anode during the high-amplitude half cycle of the AC-EPD unless specifically stated otherwise. For comparison, DNase coatings were prepared on PDA electrodes by classic dipping for 10 min in the same DNase I suspension to evaluate the surface deposition in the absence of an electric field. The latter dip-coated samples are hereafter referred to as DNase-dip.

A qualitative evaluation of the surface topography after various processing steps was performed by SEM and AFM (**Figure 2a and b)**. The morphological differences between pol-Ti and pDA-Ti surfaces confirmed the formation of a distinct PDA layer on the Ti surface. The PDA layer appeared to consist of nanoaggregates, corresponding well to the suggested deposition mechanism of PDA by Bernsmann *et al.* [67]. After 10 min of AC-EPD, extensive DNase deposits had formed covering the entire surface (DNase-EPD). In contrast, after 10 min of dipping, only fragmented deposits could be observed on DNase-dip, while the pristine PDA nanoaggregate surface appeared still visible on other parts of the surface. These results were corroborated by the quantitative surface roughness data derived from the AFM as shown in **Figure 2c**. The average surface roughness (S_a) of pol-Ti slightly increased from 5.7 nm to 6.8 nm with the formation of the intermediate PDA layer (pDA-Ti). After AC-EPD of DNase I, the S_a increased significantly to 19.9 nm, whereas the S_a after dipping (DNase-dip) amounted to only 6.3 nm. Furthermore, the coating thickness was determined after each processing step by ellipsometry (**Figure 2d**). For the native TiO_2 layer, the film thickness and the refractive index of the film were determined as 4.4 nm and 2.17, respectively. It was observed that the intermediate PDA layer had a thickness of 16.9 nm with a refractive index of 1.48. The DNase film thickness when deposited by AC-EPD (DNase-EPD) amounted 12.8 nm with a refractive index of 1.28 and a surface mass density of 0.2 ± 0.01 ng mm^{-2} as estimated using the de Feijter formula. The fragmented DNase deposit observed after dipping (DNase-dip) did not allow to obtain a physical value for the film thickness and refractive index.

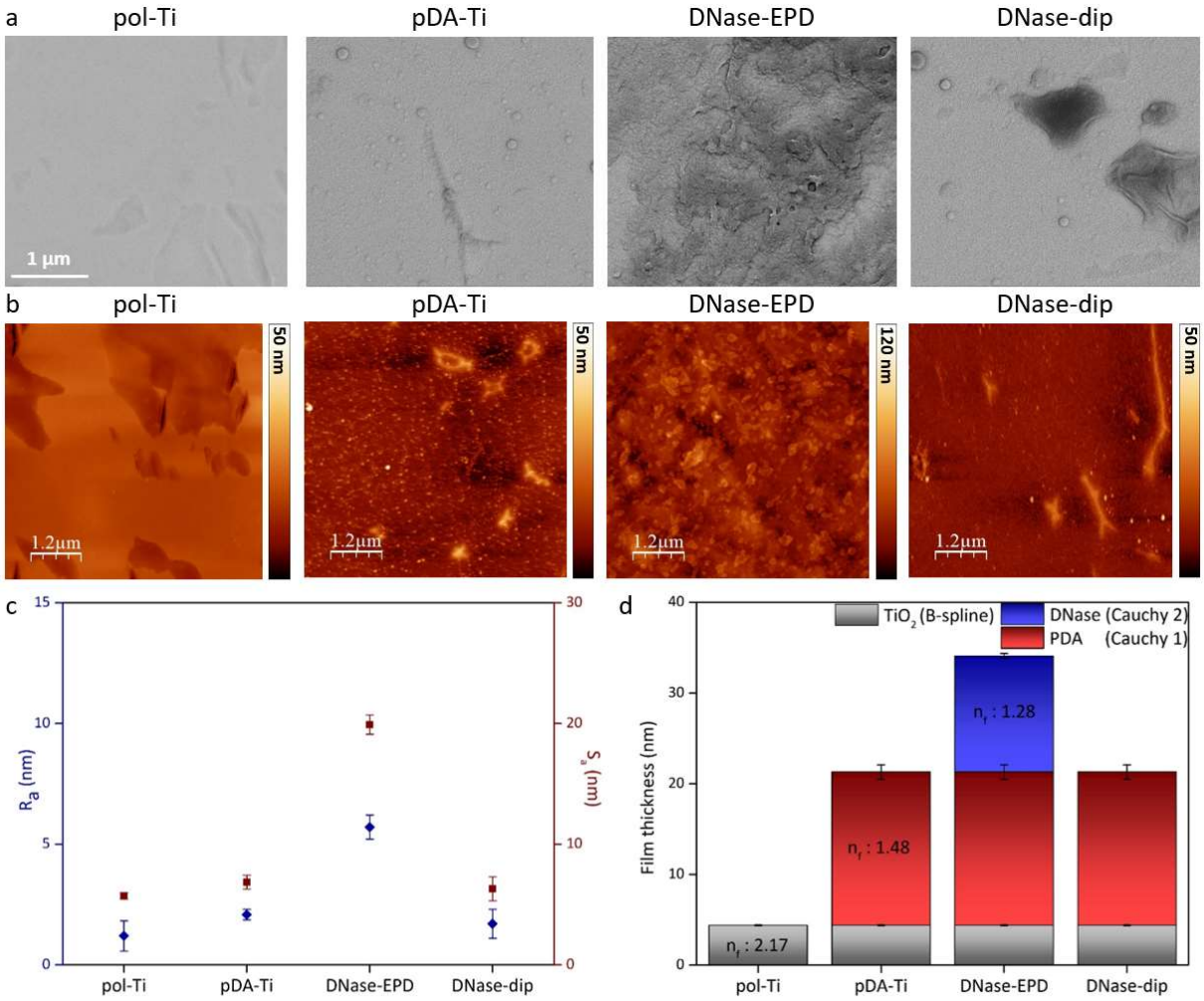

Figure 2. *Surface topography and film thickness evaluation after various processing steps in the DNase coating procedure.* (a) Representative back-scattered SEM and (b) AFM micrographs of pristine polished titanium (pol-Ti), functionalized with an intermediate PDA layer (pDA-Ti) and coated with DNase I by means of AC-EPD (DNase-EPD) or classic dipping (DNase-dip). (c) The arithmetic mean roughness (R_a) and the average surface roughness, S_a, as determined by AFM and (d) the total film thickness and refractive index, as determined by spectroscopic ellipsometry. Numerical data are presented as average ± standard deviation.

To determine the surface free energy and its dispersive and polar components of the surfaces after various processing steps in the DNase coating procedure, contact angle measurements were performed using milliQ water, ethylene glycol and diiodomethane as test liquids (**Figure 3a**). For all test liquids, the contact angle of pol-Ti decreased upon PDA functionalization (73.5 ± 1.4° vs. 54.8 ± 0.7° for milliQ H_2O, 48.5 ± 1.4°

vs. 18.9 ± 0.9° for ethylene glycol and 37.8 ± 2.6° vs. 24.8 ± 2.7° for diiodomethane). Deposition of a DNase I top layer by both AC-EPD and dipping again increased the contact angles. More precisely, water contact angles amounted 65.2 ± 1.6° and 61.5 ± 1.8°, respectively. Based on these results, the total surface free energy (γ^{tot}) and its dispersive Lifshitz–van der Waals (γ^{LW}) component and polar acid-base (γ^{AB}) component, which was derived from the electron accepting (γ^{+}) and electron donating (γ^{-}) components, were calculated (**Figure 3b**). The total surface free energy of the pol-Ti surface was 41.9 mJ m^{-2} and incorporation of a PDA layer increased the total SFE to 51.2 mJ m^{-2}. Introduction of a DNase I coating reduced the γ^{tot}, resulting in similar values for DNase-EPD and DNase-dip (41.6 mJ m^{-2} and 43.9 mJ m^{-2}, respectively). Values for the dispersive component γ^{LW} were similar for all surfaces, ranging from 38.47 to 46.2 mJ m^{-2}. The polar component γ^{AB} of pristine pol-Ti amounted only 1.1 mJ m^{-2}, which slightly increased to 5.1 mJ m^{-2} after PDA functionalization. Introduction of a DNase I coating on pDA-Ti led to comparable values for γ^{AB} for both techniques, being 3.2 and 5.2 mJ m^{-2} for DNase-EPD and DNase-dip, respectively. A more detailed analysis of the polar component to reveal the electron accepting/donating behavior of the surfaces showed that for all surfaces γ^{+} was below 0.4 mJ m^{-2}, while γ^{-} ranged from 10.2 to 20.4 mJ m^{-2}, indicating monopolar surfaces with electron-donor capacity [52]. The surface of pol-Ti showed the lowest γ^{-} value compared to treated surfaces owing to the nonpolar nature of the metal oxide surface [68].

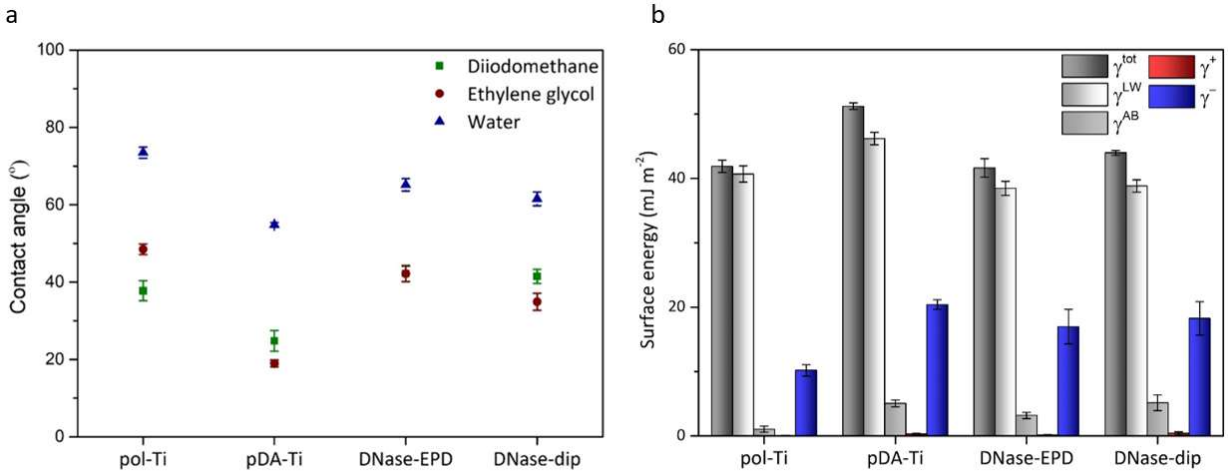

Figure 3. *Surface wetting behavior after various processing steps in the DNase coating procedure.* (a) Contact angles for water, ethylene glycol and diiodomethane and (b) the calculated total surface free energy (γ^{tot}) and its dispersive Lifshitz-van der Waals (γ^{LW}), polar acid-base (γ^{AB}), electron accepting (γ^{+}) and electron donating (γ^{-}) components for pristine polished titanium (pol-Ti), functionalized with an intermediate PDA layer (pDA-Ti) and coated with DNase I by means of AC-

EPD (DNase-EPD) or classic dipping (DNase-dip). Data are presented as average ± standard deviation.

XPS analyses were performed to evaluate the surface chemical composition of the experimental surfaces, overlay plots of survey spectra as well as high-resolution spectra for C 1s, N 1s, and O 1s are shown in **Figure 4**, while quantitative data are summarized in **Table 1**. Detailed deconvoluted high-resolution spectra for C 1s, N 1s, and O 1s of are provided in the Supporting Information, **Figure S4**. The pristine pol-Ti exhibited strong carbon (C 1s) and oxygen (O 1s) signals, which might be attributed to an over-layer of ambient carbon contaminants [69]. Following PDA functionalization, a drastic reduction of the Ti (Ti 2p) substrate signal (from 13% to 1%) was observed accompanied by a substantial increase in carbon (from 36% to 69%) and in nitrogen (N 1s) (from 0% to 7%), indicative of a distinct layer of PDA. Indeed, the PDA layer thickness of 16.9 nm (as confirmed by ellipsometry above) is larger than the XPS information depth (~5 nm), so that only a small Ti 2p peak positioned at 456 eV was visible in the survey scan. Introduction of a DNase I coating further reduced the Ti signal, while the amount of nitrogen increased, this effect was more pronounced for coatings prepared by AC-EPD (i.e. DNase-EPD anode) than for coatings obtained by classic dipping (i.e. DNase-dip). This suggests that DNase-EPD anode coatings are thicker or more homogeneous, which is in agreement with the results obtained from SEM and AFM above where DNase-EPD anode coatings appeared thicker. For a more in-depth comparison of the chemical bonding present in each sample, an overlay of the relevant high-resolution spectra is given in **Figure 4**, while details of the peak deconvolution are summarized in **Figure S4**. The C 1s spectrum of the pDA-Ti surface in **Figure S4a** (on the left) was deconvoluted into three peak components, a peak at 288.2 eV was attributed to the C=O, one at 286.1 eV, which was assigned to C-O and C-N, and one at binding energy 284.6 eV, attributed to C-H and C-C species in the PDA structure [70,71]. For surfaces that were in contact with DNase I (DNase-EPD anode, cathode and DNase-dip), a peak at binding energy around 288.0 eV with a 0.1 eV deviation depending on the exact sample (**Figure S4b-d**, on the left, on the high-energy side), which can be attributed to the peptide bond –C(=O)-NH_2 and is indicative for proteins [72,73]. The peak intensity fraction of this peak around 288.0 eV for DNase-treated samples was varying between 17% (DNase-EPD anode) and 13% (DNase-EPD cathode), which indicates a thicker DNase deposit on the anode. For DNase-dip, the peak intensity fraction of the peak at 288.0 eV was 12%. Based on the proposed chemical structure of the PDA layer, the N 1s region (**Figure S4a-d,** in the middle) was deconvoluted into three peak components corresponding to primary (R-NH_2 at 401.5 eV), secondary (R-NH-R at 399.8 eV), and tertiary (=N-R at 398.5 eV) amine functionalities of pDA-Ti sample [74]. In the O 1s region (**Figure S4a-d,** on the

right), two peaks could be fitted to all samples, a peak at higher binding energy representing the O-C bond, and another peak representing the O=C bond [74]. Interestingly, the contribution of O 1s signal components was different for pDA-Ti than for DNase-treated samples. For pDA-Ti, the O 1s signal was composed of ~39% O=C and ~61% O-C. However, in DNase-treated samples, i.e. DNase-EPD anode, DNase-EPD cathode and DNase-dip, the O=C bond contributed with ~77%, ~67%, and ~52%, respectively, while the O-C contribution amounted ~23%, ~33% and ~48%, respectively.

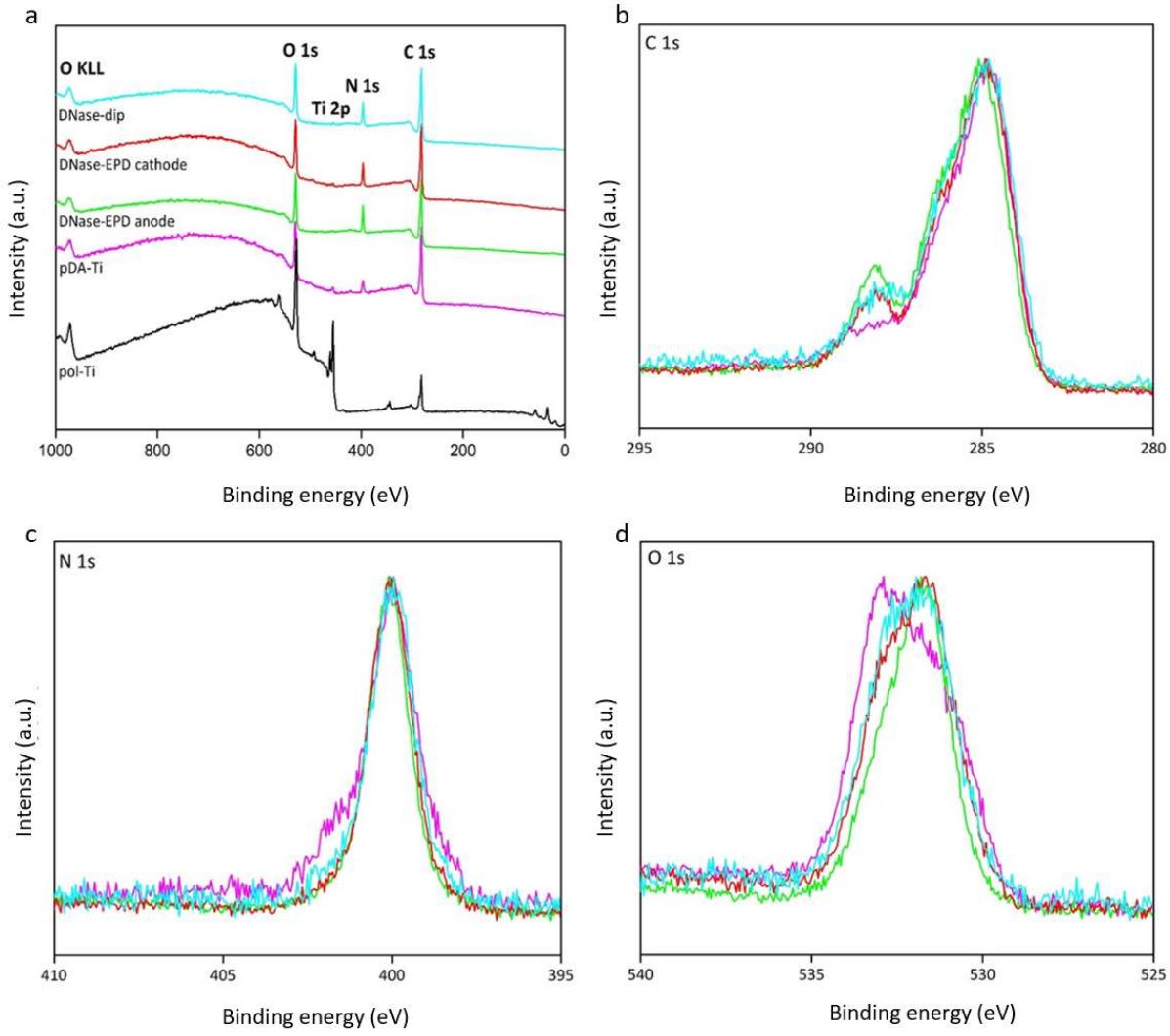

Figure 4. *XPS spectra of Ti substrates after various processing steps in the DNase coating procedure.* (a) wide-scan survey spectra of pristine titanium (pol-Ti), PDA functionalized Ti (pDA-Ti), coated with DNase I by means of AC-EPD (DNase-EPD anode and DNase-EPD cathode, respectively) and coated with DNase I by classic dipping (DNase-dip), (b) high-resolution of C 1s spectrum, (c) N 1s

spectrum, (d) O 1s spectrum for pDA-Ti, DNase-EPD anode, DNase-EPD cathode and DNase-dip, respectively.

Table 1. *Surface elemental composition of Ti substrates after various processing steps in the DNase coating procedure.* Quantitative XPS analysis of carbon, nitrogen, oxygen and titanium for pristine polished titanium (pol-Ti), functionalized with an intermediate PDA layer (pDA-Ti) and coated with DNase I by means of AC-EPD (DNase-EPD anode, DNase-EPD cathode) or classic dipping (DNase-dip).

At%	**O**	**C**	**N**	**Ti**
pol-Ti	51	36	0	13
pDA-Ti	23	69	7	1
DNase-EPD anode	20	67	13	0
DNase-EPD cathode	21	68	11	0
DNase-dip	22	66	12	0

In addition, ToF-SIMS measurements in combination with a PCA were conducted to clarify the surface chemistry of pristine and coated Ti substrates. The used peak list contained fragments characteristic for proteins [55], PDA and the Ti substrate (**Table S1**). The positive polarity ToF-SIMS spectra of the Ti substrates after various processing steps were fitted with this peak list and subjected to PCA. **Figure S5** shows the first two principal components (PC), which together capture a spectral variance of 91%. A distinct change in surface composition could be observed after the various processing steps. PC1 clearly separated the pol-Ti substrate from the remaining samples (**Figure S5a**). The signals related to the Ti reference mainly resulted from Ti/TiO_x^+, salts and carbohydrates, which loaded negatively in PC1, while all PDA and protein characteristic fragments loaded positively in PC1. All samples that came in contact with the DNase suspension contain amino acid fragments and consequently separated clearly from the protein-free samples. Hydrophobic amino acid residues, such as phenylalanine (Phe) and valine (Val), were also detected by ToF-SIMS (**Figure 5b**). The presence of exposed hydrophobic amino acid residues at the coating surface can render increase the hydrophobicity, which is in agreement with the observations from the contact angle measurements. Interestingly, DNase-EPD cathode samples were less homogeneous compared to the remaining sample types, reflected by a higher variation in the scores, and showed a trend towards the pDA-Ti samples. In PC2, the captured variation related to the signals of PDA, emphasizing the characteristics of the PDA layer (**Figure S5b**). In addition, some aromatic and nitrogen containing fragments loaded positively with the PDA samples, which are possible fragments of a PDA polymer.

To elucidate possible differences between DNase-coated surfaces in more detail, a PCA was conducted only taking into account sample types that were in contact with DNase (DNase-dip, DNase-EPD anode and cathode, respectively) (**Figure 5**). The ToF-SIMS analysis showed clear amino acid fragments for all samples. Given that the information depth of the technique is in the range of 1-3 nm, these results indicate that at least a monolayer of DNase I adsorbs to the substrate in all of these conditions. No significant difference in disulfide signals (S_2^-; values related to the peptide bond CNO^- are 0.0070 ± 0.0003 for DNase-dip, 0.0063 ± 0.0004 for DNase-EPD cathode and 0.0072 ± 0.0003 for DNase-EPD anode, respectively) was observed, suggesting that the tertiary protein structure is not influenced by the method of deposition [75]. The DNase-EPD cathode could be clearly distinguished from the DNase-EPD anode and DNase-dip samples and showed the lowest homogeneity and the highest variation within the spectra of the same sample type. The observed variance was mainly caused by PDA-related fragments, suggesting either a thinner or more patchy protein coating on the DNase-EPD cathode. PCA with an ion-containing peak list (as in Table S1, not shown) suggested that ionic signals (e.g., Na^+, K^+) correlated mainly with the DNase-EPD cathode. Both DNase-dip and DNase-EPD anode samples clearly related to the amino acid fragments. The DNase-EPD anode scored even more negatively than the DNase-dip samples, indicating a denser and more complete protein coverage for the AC-EPD method.

Overall, the here presented data from the different characterization techniques indicate that AC-EPD can be a versatile tool to increase the enzyme adsorption on PDA-functionalized Ti metal substrates.

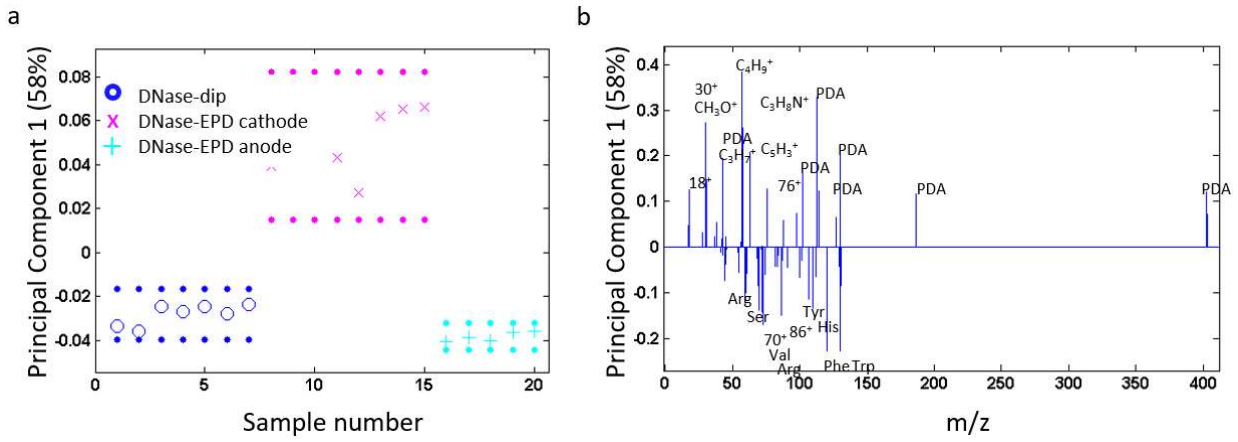

Figure 5. *PCA results of ToF-SIMS spectra for samples in contact with DNase I.* (a) Scores plot on PC1 with (b) corresponding PC1 loadings (all signals above a threshold of 0.1 are labelled, signals corresponding to multiple fragments are labeled with their mass) plot for PDA-functionalized titanium substrates after treatment with DNase I by means of AC-EPD (DNase-EPD anode and

cathode, respectively) or by classic dipping (DNase-dip). PC1 separates the DNase-EPD cathode (i.e. counter electrode) from the DNase-EPD anode (i.e. working electrode) and DNase-dip samples.

3.2. AC-EPD deposition translates to an elevated DNase activity at the Ti surface.

Following deposition optimization for DNase-EPD and DNase-dip, the enzymatic activity of the DNase-coated Ti surfaces was assessed using a recently developed qDNase assay (**Figure 6a**) [57]. For freshly prepared coatings, the surface activity was threefold higher when coating was performed 10 min by AC-EPD compared to dipping (i.e. 118.95 ± 19.36 mU for DNase-EPD and 37.01 ± 18.51 mU for DNase-dip). Taking into account the total activity of the DNase suspension (i.e. 35 U), this corresponded to an activity yield of 0.34% and 0.11% for DNase-EPD and DNase-dip, respectively. For comparison, the surface activity of DNase-dip(6h), prepared as reported previously by classic dipping for 6 h at room temperature [34,36,37], was significantly lower (i.e. 2.44 ± 0.38 mU), corresponding to an activity yield of only 0.01% as compared to the original DNase suspension. Fast deposition by AC-EPD and classic dipping thus resulted in a significantly higher activity of the coated surfaces, i.e. 49-fold and 15-fold respectively.

To assess whether coated enzymes remained active over a longer storage period, which could be relevant for practical applications, samples were dried, kept at 4°C and assessed for surface activity after 1, 3 and 7 days (**Figure 6b**). Activity of both DNase-EPD and DNase-dip gradually reduced over time due to denaturation, but still retained 32.13% and 36.74% of the corresponding initial surface activity after seven days. Similarly to what was observed for the fresh coating activity, DNase-EPD was more active than DNase-dip at each time point.

Finally, to gain insight in the nature of the DNase tethering to PDA-coated Ti, the release profile of DNase activity from the coated surfaces into PBS was measured over a period of 24 h (**Figure 6c**). For DNase-dip, approximately all activity was released in a high burst within the first 2 h of the experiment, after which no more release was detected. For DNase-EPD, a rapid release of approximately 75% of the activity was detected within the first 2 h of the experiment, followed by a slower sustained release in the following hours. After 24 h, a total of 57.6 ± 12.5 mU and 19.6 ± 5.0 mU was released from the DNase-EPD and DNase-dip surfaces, respectively. The remaining surface activity at this time point was 1.58 ± 0.12 mU and 0.38 ± 0.04 mU, corresponding to 1.33% and 1.02% of the initial surface activity of DNase-EPD and DNase-dip, respectively (**Figure 6d**).

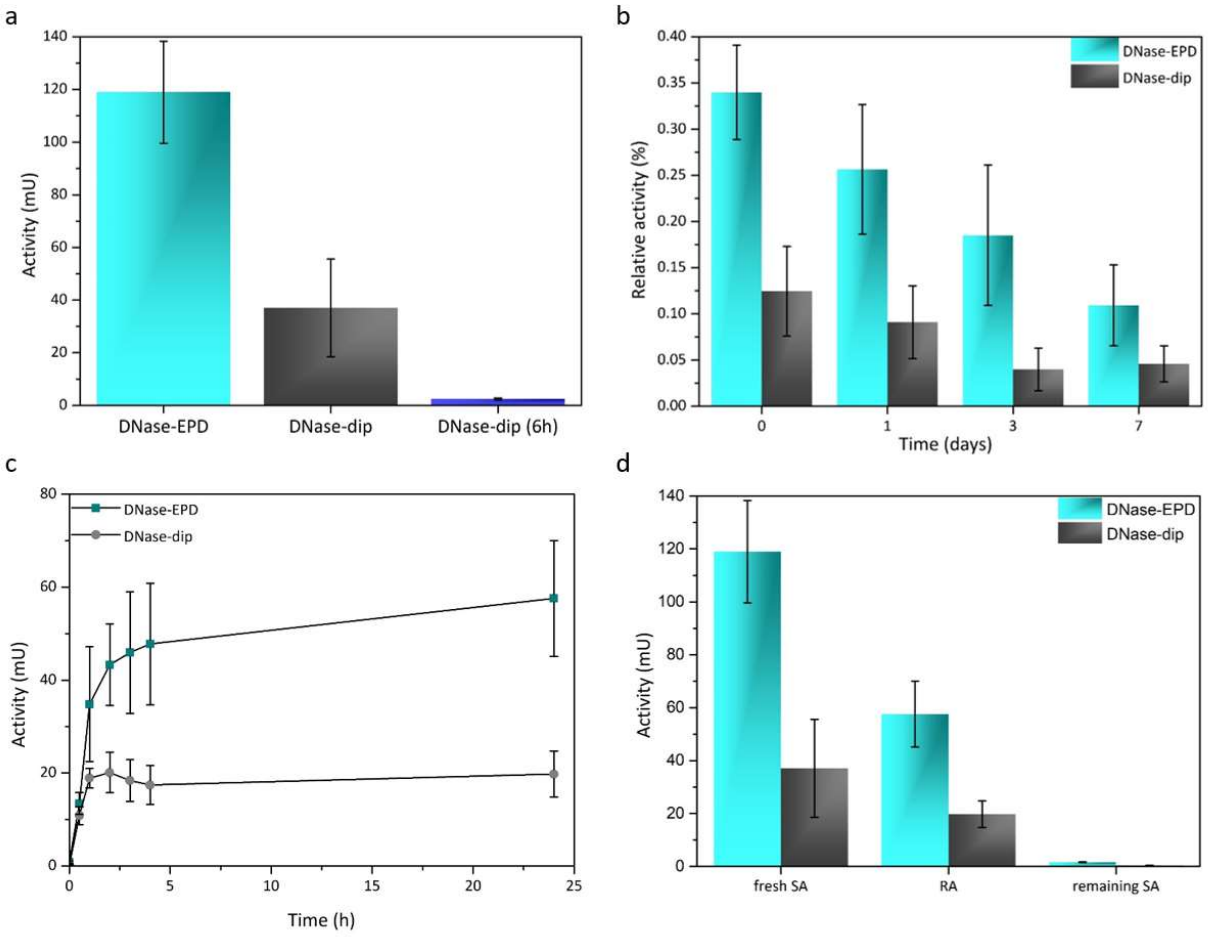

Figure 6. *Activity assessment of DNase I coatings obtained by AC-EPD and classic dipping.* (a) Fresh surface activity. DNase coatings prepared by classic dipping for 6 h (DNase-dip (6h); dark blue) were used as reference. (b) Surface activity after dry storage at 4°C for 0, 1, 3 and 7 days. (c) DNase release profile representing the cumulative released DNase activity from the coatings over 24 h into PBS at 4°C. (d) Distribution of DNase activity of coatings: fresh surface activity (SA), total released activity (RA) over 24 h into PBS at 4°C, remaining SA after 24 h immersion in PBS at 4°C.

3.3. DNase I coatings processed by AC-EPD inhibit *in vitro* biofilm formation more efficiently than dip-coated DNase.

As a final step, the *in vitro* anti-infective properties of the DNase-coated Ti discs were studied. To achieve this, biofilms were grown for 20 h on the different substrates using two predominant implant infection-associated species: *S. epidermidis* and *P. aeruginosa.*

Initially, an explorative, visual analysis of the biofilms was performed by SEM (**Figure 7a, 8a**, **S6a, S7a**). Both DNase-EPD and DNase-dip visibly inhibited biofilm formation of both species compared to the controls, i.e. pol-Ti and pDA-Ti. While only a limited amount of bacterial cells was present on the DNase-coated Ti, a rather thick, 3D-like community of bacteria adhered to the controls. An exception to this were the *P. aeruginosa* biofilms on pol-Ti, where only a few cells adhered to the substrate. As the biofilm preparation protocol for biofilm fixation for SEM included a number of washing steps, a significant amount of cells was likely washed off. Therefore, CLSM was used as a second biofilm analysis approach, as it included fewer washing steps.

The 20 h-old biofilms of both species on the different substrates were LIVE/DEAD® stained and imaged by CLSM (**Figure 7b, 8b**, **S6b, S7b**). This time, visual analysis of the CLSM images showed that significant biofilms were present on all pol-Ti and pDA-Ti samples. Moreover, biofilm formation was visibly reduced on DNase-coated samples. This was more pronounced for DNase-EPD compared to DNase-dip, pointing towards a stronger inhibitory effect of DNase-EPD compared to DNase-dip on biofilm formation. Nonetheless, substantial variation in biofilm adhesion could be observed on the different substrates (**Figure S6b, S7b**).

To enable a more objective comparison, several biofilm parameters were quantified; i.e. the biovolume, the average biofilm thickness over the observed area, average biofilm thickness over biomass-covered area, maximum biofilm thickness, number of microcolonies and average volume of microcolonies (**Figure 7c-e, 8c-e**). Although quantification confirmed the high variability in biofilm formation, several insights could be obtained. First, biofilm formation was consistently lower on pol-Ti than on pDA-Ti. Subsequently, the impact of DNase coatings was compared to both pol-Ti and pDA-Ti. Second, biofilms of both species on DNase-EPD showed significant reductions for principal parameters including biovolume, average biofilm thickness over the observed area, number of adhering microcolonies and average volume of microcolonies. In contrast, DNase-dip only significantly reduced the number of microcolonies and average volume of microcolonies of *S. epidermidis* biofilms, albeit to a lower extent, and no biofilm characteristics of *P. aeruginosa*. Finally, for two parameters, i.e. average biofilm thickness over biomass-covered area and the maximum biofilm thickness, no significant reductions were detected for both DNase coatings, when compared to the controls (**Figure S6c-d, S7c-d**). Overall, these results indicate that DNase coatings prepared by EPD are more effective to inhibit biofilm formation over a 20 h time period than DNase coatings prepared by dipping and this for the same duration of the coating procedures.

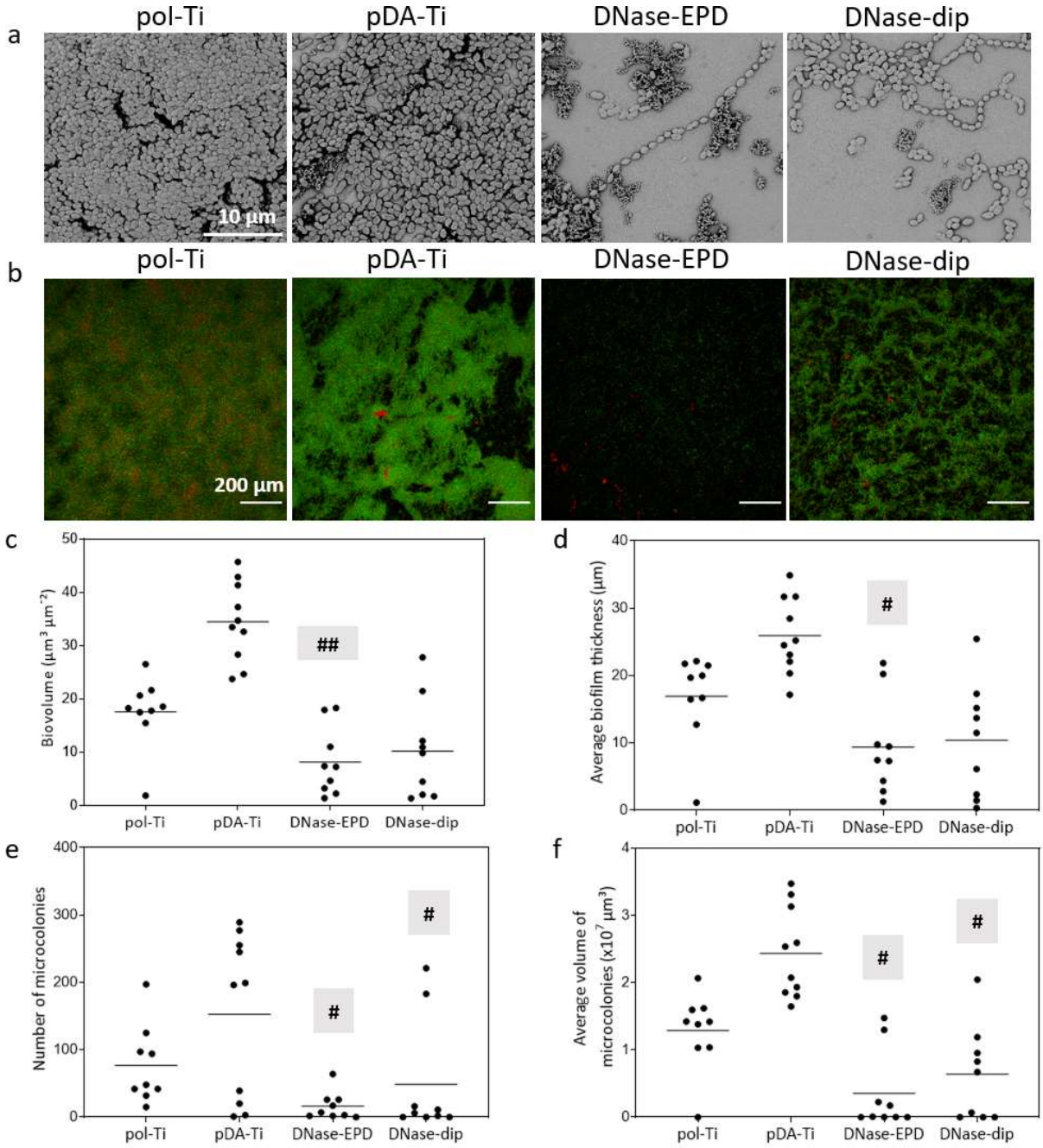

Figure 7. *In vitro anti-infective activity of different Ti substrates against 20 h-old Staphylococcus epidermidis biofilms.* (a) Representative SEM visualization of biofilms. Scale bars correspond to 10 µm. (b) Representative CLSM image stacks of biofilms. Live bacteria are stained green, while dead bacteria are stained red. Scale bars correspond to 200 µm. (c) Biovolume, (d) average biofilm thickness over the observed area (e) number of adhering microcolonies and (f) average volume of adhering microcolonies. . Dots represent the data points retrieved from three image stacks on three replicate discs inoculated with independent bacterial inoculums. Horizontal lines represent

the average. Significant differences in biofilm parameter of DNase-coated substrates (DNase-EPD or DNase-dip) compared to both negative controls (pol-Ti and pDA-Ti) are highlighted ($^{\#}p < 0.05$; $^{\#\#}p < 0.01$).

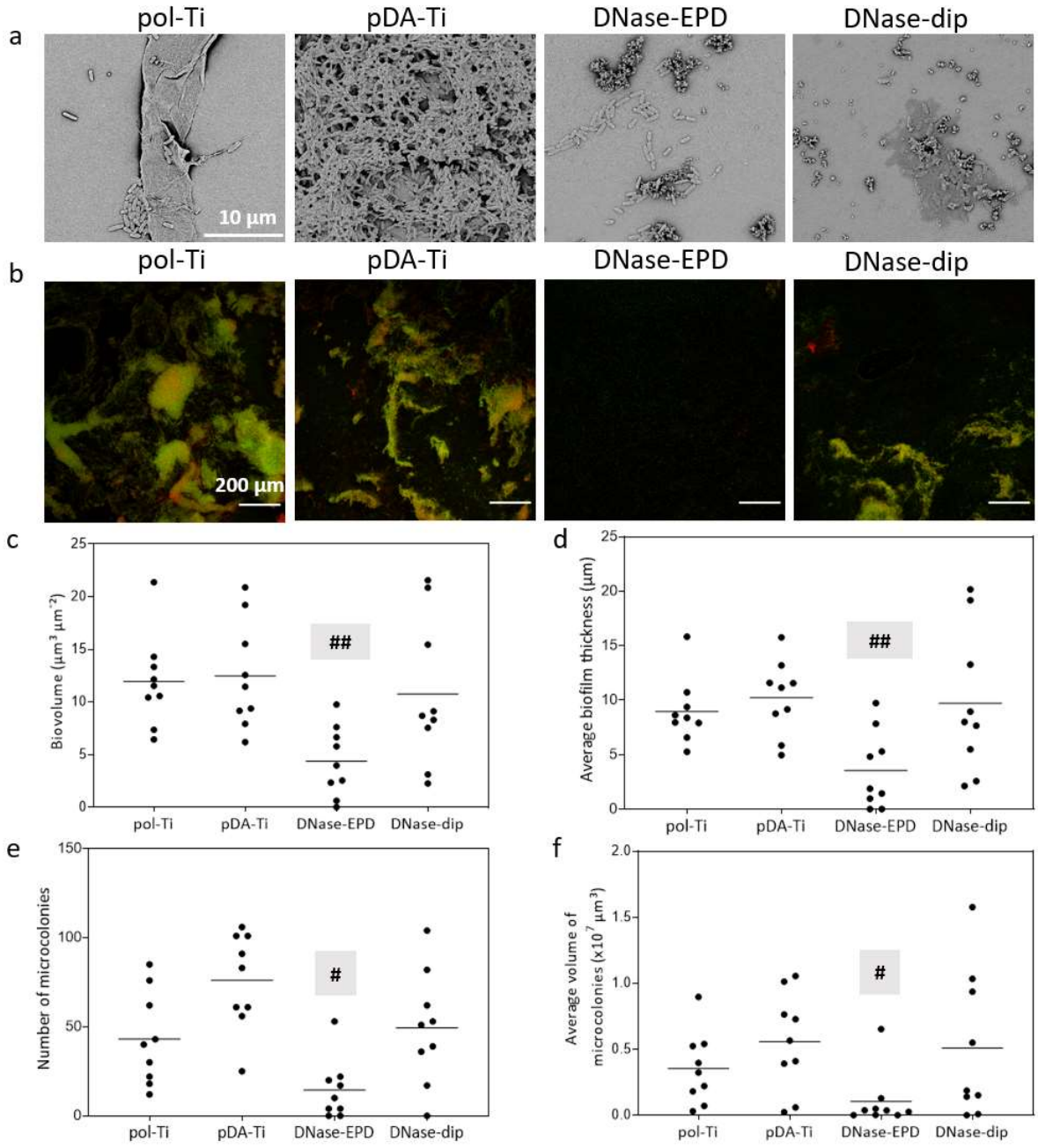

Figure 8. *In vitro anti-infective activity of different Ti substrates against 20 h-old Pseudomonas aeruginosa biofilms.* (a) Representative SEM visualization of biofilms. Scale bars correspond to 10 µm. (b) Representative CLSM image stacks of biofilms. Live bacteria are stained green, while dead

bacteria are stained red. Scale bars correspond to 200 µm. (c) Biovolume, (d) average biofilm thickness over the observed area (e) number of adhering microcolonies and (f) average volume of adhering microcolonies. Dots represent the data points retrieved from three image stacks on three replicate discs inoculated with independent bacterial inoculums. Horizontal lines represent the average. Significant differences in biofilm parameter of DNase-coated substrates (DNase-EPD or DNase-dip) compared to both negative controls (pol-Ti and pDA-Ti) are highlighted ($^{\#}p < 0.05$; $^{\#\#}p < 0.01$).

4. Discussion

Several research groups have independently shown that DNase coatings can prevent biofilm formation on a variety of surface-functionalized medical implants [34–37]. All the reported DNase coatings were previously prepared by classic dipping, a diffusion-controlled immobilization process. This strategy requires long processing times, which may result in a significant loss of enzyme activity. To address these hurdles, we hypothesized that AC-EPD can be used as a fast alternative immobilization strategy to prepare anti-infective DNase coatings on PDA-functionalized Ti implants with an improved enzymatic activity [47]. Therefore, in this study DNase coatings were immobilized for 10 min by both AC-EPD and classic dipping and were compared in terms of surface characteristics, enzymatic activity and anti-infective properties.

The driving force for particle, and therefore also macromolecule, movement in an external electric field is its surface charge and electrophoretic mobility in the solvent [76]. It is generally accepted that the zeta potential, as a measure of the surface charge, should have an absolute value of at least 30 mV to enable migration during EPD. Proteins in water develop a charge through the ionization of the amino acid functional groups exposed at the surface, which can change in function of the medium pH. Although **Figure S2** suggests that it is possible to fine-tune the DNase zeta potential within the target range for EPD by changing the suspension pH, care should be taken not to alter the degree of ionization of the amino acids too much as this can induce enzyme denaturation and hence deactivation of the enzyme at too high or low pH. The optimal pH range ensuring maximum activity of DNase I is around pH 6.5-8 [77]. However, adjusting the pH to increase the zeta potential will also lead to an increase in the ionic strength of the medium which further elevates the risk of water electrolysis [40]. For this reason, AC-EPD processing was performed at the natural pH of the suspension, i.e. ~6.5.

Moreover, the AC-EPD process itself also entails a risk of enzyme inactivation, due to possible pH and temperature changes during AC electrolysis [78]. As such, it has been shown before for voltage-controlled

AC-EPD of glucose oxidase that limiting the amplitude of the AC signal while increasing the frequency allows maintaining active enzyme coatings [78]. However, a similar trend could not be observed in the current study owing to the high variability observed for the surface activity (**Figure S3a**). Indeed, at relatively low peak-to-peak amplitude (i.e., 0.75, 1.5 and 3 mA cm^{-2}, respectively), a high variability in enzyme activity was measured, which could be because of the resuspension of weakly deposited molecules upon field reversal of the applied AC signal. On the other hand, higher peak-to-peak amplitudes either resulted in a decreased enzyme activity or a higher variability, which might be attributed to water electrolysis (and concomitant Joule heating and pH shifts) associated with high-amplitude asymmetric AC signals [40,78]. As a result, the highest repeatability for DNase I coatings processed by means of current-controlled AC-EPD was observed for an intermediate peak-to-peak current value of 6 mA cm^{-2} at a frequency of 100 Hz. Nevertheless, the highest activity was observed on the electrode coupled as anode during the high-amplitude half cycle, while only a reduced activity was observed on the cathode (**Figure S3b**). These observations are in agreement with our previous findings for AC-EPD of BSA, where it was hypothesized that the macromolecules migrate more effectively during the high-amplitude half cycle than during the low-amplitude half cycle [47]. Correspondingly, here as well, the negatively charged DNase I has a higher deposition yield on the positively charged electrode, i.e. anode, during the high-amplitude half cycle.

When comparing the AC-EPD and dip-coating methods for the same processing time by means of SEM and AFM, remarkably larger deposits were observed on DNase-EPD anode samples than DNase-dip (**Figure 2a-b**). This was also confirmed by thickness measurements using ellipsometry, which indicated that a 12.8 nm thick DNase coating was achieved by AC-EPD, while after dip-coating no appreciable layer thickness could be determined (**Figure 2d**). This was also supported by the XPS data, clear signals at 288.0 eV associated with protein peptide bonds –C(=O)-NH_2 were observed in the XPS C 1s high-resolution spectra for the samples that were in contact with DNase I, but DNase-EPD anode showed the highest peptide bond content (**Figure 4b** and **Figure S4**, left). A peak at 288.2 eV was also observed on pDA-Ti substrate, yet can be assigned to C=O found in the quinone structure of PDA [70]. High-resolution O 1s spectra indicated a different chemical environment for PDA-functionalized substrate (pDA-Ti) and the DNase-treated samples (**Figure 4d, Figure S4a-S4c,** on the right). As such, the contribution of the two bonds to the O 1s peak, i.e. O-C and O=C, showed a drastic difference between PDA and DNase-treated samples. When comparing DNase-treated samples, the intensity of the O-C bond was higher in DNase-EPD cathode and DNase-dip samples compared to DNase-EPD anode, which can be attribute to more intense PDA substrate signals due to a thinner protein layer. These results are corroborated by the ToF-SIMS data, which show more

pronounced PDA substrate signals on the electrode coupled as cathode, indicative of a thinner deposit (**Figure 5**). Yet, clear DNase I protein signals were also observed by ToF-SIMS for both DNase-EPD anode and DNase-dip, suggesting that at least a monolayer of DNase I is present at the surface after both coating methods (**Figure 5**). Still, also the ToF-SIMS analyses pointed at a denser DNase I deposit on DNase-EPD samples then seen for DNase-dip. Overall, these results confirm that AC-EPD accelerates the DNase I enzyme coating procedure as compared to conventional dip-coating for the same process duration.

Besides the improved surface coverage, which is a prerequisite in order to ensure a good spatial distribution of the DNase anti-infective activity, DNase-EPD coatings also present beneficial surface properties to support host tissue cell interactions. Nano-scale topography has been reported to promote protein adsorption and subsequent cell adhesion [79–81]. Here, it could be noted that the additional layer formed on DNase-EPD samples significantly increased the surface roughness, while for DNase-dip, values were similar as for pristine pol-Ti or pDA-Ti surfaces (**Figure 2c**). Therefore, it can be expected that the higher S_a value of DNase-EPD samples will contribute to a better cell adhesion as compared to DNase-dip reference substrates. In addition, the surface hydrophilicity was reduced by the introduction of the DNase I coatings, which might be attributed to the presence of exposed hydrophobic amino acid residues, such as phenylalanine (Phe) and valine (Val), as detected by ToF-SIMS (**Figure 5b**) [82]. This can be of interest for anti-infective coating applications, as it has been reported that the hydrophobic amino acid substitutions are effective to inhibit bacterial growth [83]. Furthermore, also the SFE components changed with various steps in the DNase I coating process. For pristine pol-Ti, the total SFE (γ^{tot}) is dominated by the apolar component (γ^{LW}), while the polar electron donor (γ^{-}) and acceptor (γ^{+}) components do not contribute significantly. The electron donor capacity, however, was improved through incorporation of the intermediate PDA layer, which can be associated with the addition of electron donating amine groups [84,85]. Surprisingly, there was a slight increase in electron acceptor (γ^{+}) functionality on DNase-dip. This might be attributed to the presence of cations, such as Ca^{2+}, a known electron acceptor, as was detected by ToF-SIMS as well (**Table S1**) and which have been suggested to contribute to the enzymatic activity of DNase I [52,86]. DNase-EPD coatings showed a lower electron acceptor behavior, which might be attributed to the absence of these cations, as also indicated by ToF-SIMS analysis. However, this did not translate to a reduced enzymatic activity. On the contrary, DNase-EPD coatings showed an increased activity when compared to DNase-dip (**Figure 6**), but this can maybe be attributed by the improved surface coverage of DNase-EPD coatings.

The key to the anti-biofilm properties of DNase I lies in its enzymatic activity [87–89]. In this regard, the DNase I immobilization processes should be optimized to maintain maximum enzymatic activity. We recently published a new method to quantify DNase I activity on coated surfaces in real time, called qDNase assay, which was used here to quantify and compare different enzymatic properties of the DNase I coatings [57]. It should be noted that for all the activity assays, no straightforward relationship between amount of DNase I and its corresponding activity is observed, for multiple reasons. First, the assays only measures the activity of DNases which are exposed to the substrate solution, meaning that DNases that are still tethered to the surface and covered by superimposing DNase I layers potentially do not contribute to the observed activity. Furthermore, like all suspended proteins, DNase I released into PBS tends to stick to surfaces like the polystyrene microplate, lowering the bulk concentration and consequently the measured released activity [90]. Finally, like all proteins, DNase I becomes inactivated over time. This was also demonstrated in **Figure 6b**. Taking this into account, the activity assays cannot simply be used to estimate the total amount of deposited and released DNase I. Rather, they should be interpreted as the 'accessible activity' to substrate and consequently to eDNA during biofilm formation, which is most relevant for the application as anti-infective.

Fresh AC-EPD-coated surfaces were threefold more active than dip-coated surfaces prepared with the same deposition time (**Figure 6a**). As ToF-SIMS data indicated that for both coating techniques at least a DNase I monolayer was present, it could indeed be expected that the accessible surface activity would be within the same order of magnitude. The observed higher fresh surface activity of the EPD coatings either results from a higher surface roughness and therefore higher specific surface area of the DNase I deposits, as indicated by AFM, or from the presence of more additional loosely deposited DNases, which were already released during the assay. Released DNases potentially provide an additional benefit to the anti-infective coating as they might act on eDNA that is not exposed directly to the surface, but rather contributes to further biofilm expansion at more distal sites.

Interestingly, DNase I coated surfaces were significantly more active when prepared by 10 min deposition time than with the previously reported 6 h classic dipping protocol (**Figure 6a**). This supports the hypothesis that long immersion times can result in significant losses of enzyme activity. Moreover, surfaces of both DNase-EPD and DNase-dip remained active after storage for 7 days at 4°C, while for 6 h-dipped samples[37] activity was previously reported to last only up to 16 h under these storage conditions (**Figure 6b**). These findings justify the use of shorter deposition times to ensure high enzymatic activity of DNase I coatings.

Release studies suggest that, independent from the used coating technique, only a small fraction of the DNases stably immobilizes on the surface, whereas the majority of DNase I is not permanently retained (**Figure 6c-d**). These findings are consistent with the expectations for immobilization on PDA-activated surfaces: a first layer of enzymes attaches permanently to the PDA layer on the surface by covalent bonding, whereas additional enzyme layers attach to the underlying DNase I layers through weak intermolecular interactions. The prolonged, slower release of DNase I following the high burst release, only observed for AC-EPD, probably results from the presence of the thicker DNase I deposits. Overall, this distribution of DNase I activity could be advantageous from an application perspective. Prosthetic joint infections are generally caused by bacteria that are introduced during surgery [18]. At this time, implants are most prone to bacterial attachment. However, subsequent implant covering by host cells decreases the risk of bacterial attachment [91]. This was recently demonstrated by Shield *et al.* (2020) using an *in vivo* orthopedic implant rat model. Within the first day after surgery, implants were most prone to infection. In the following days, sensitivity to bacterial colonization reduced, coinciding with an increasing number of host cells adhering to the implant [92]. Consequently, implant success can potentially increase when bacterial attachment is prevented during the first day after implantation. A high burst release of DNase I short after implantation could therefore potentially provide high short term protection. Subsequent slower release from an EPD coating might sustain this protection in the close vicinity of the surface during the first day after implantation, while the remaining permanently attached DNase monolayer potentially provide a longer lasting surface protection.

To assess the broad spectrum anti-infective performance of the coatings, biofilms were grown for 20 h on the different coatings with two relevant implant infection-related species, *S. epidermidis* and *P. aeruginosa*. Based on CLSM imaging, different characteristics of the biofilms could be extracted (**Figure 7-8**). For two biofilm characteristics, average biofilm thickness over biomass-covered area and maximum biofilm thickness, no significant reductions could be observed for both DNase-EPD and DNase-dip. Most probably, at locations on the surface with low DNase activity, biofilms could still develop without limitation achieving a local thickness similar to surfaces without DNase.

DNase-EPD is more effective than DNase-dip at inhibiting *P. aeruginosa* biofilm formation, as significant reductions in several biofilm characteristics were only measured for DNase-EPD and not for DNase-dip. The reduced biovolume and average thickness over the observed area highlights a global average reduction in adhering bacteria. Moreover, a reduction in the number of microcolonies suggests a widespread distribution of DNase activity over the DNase-EPD surface. The significantly smaller volume of

the microcolonies on DNase-EPD presumably results from surface exposed DNases that delay attachment on the surface combined with released DNases that reduce expansion of the biofilm at more distal sites.

In contrast, DNase-dip did not have any significant effect in *P. aeruginosa* biofilms. This could be due to the lack of a longer-lasting DNase release from DNase-dip, which might reduce the ability to control biofilm expansion. Moreover, as the anti-biofilm effect of DNases is dose-dependent [93], the lower activity of DNase-dip coatings compared to DNase-EPD could also contribute to the reduced anti-infectivity. However, it was previously reported that DNase coatings prepared by classic dipping for 6 h were effective to inhibit biofilm formation [34,37] and we found DNase-dip (6h) has a significantly lower fresh surface activity in the qDNase assay. This discrepancy might be attributed to assay-specific parameters including duration of biofilm growth, inoculum size and used species, or coating differences, such as a difference in distribution of the activity. Finally, a different spatial distribution of the DNase activity over the surface of DNase-dip compared to DNase-EPD could also reduce the anti-infectivity. Although ToF-SIMS data indicate that at least a DNase monolayer covers the DNase-dip surface, SEM and AFM reveal fragmented DNase deposits. Possibly biofilm formation could initiate at regions of reduced DNase activity.

Interestingly, the difference in anti-infectivity between DNase-EPD and DNase-dip is less pronounced for *S. epidermidis* biofilms. Indeed, DNase-dip significantly reduced the number of microcolonies and their average volume, although this did not result in significant reduction of the global biofilm characteristics (biovolume and average thickness over the observed area). This could potentially indicate a strain-specific difference. While the presence of eDNA is widespread among biofilms of many different species, its role in biofilm formation is time-, species- and even strain-specific [31]. Our findings indicate that biofilms of this *S. epidermidis* strain can be inhibited by DNases, but pre-formed mature biofilms of this strain were previously reported to be insensitive to DNase treatment [94]. This suggests that eDNA plays a prominent role in surface attachment of the used strain, but eDNA is reduced or less accessible during further biofilm expansion. Possibly DNase-EPD and DNase-dip are both able to prevent biofilm initiation at the surface due to coated DNases, while the additional benefit of a sustained release of DNase activity from DNase-EPD is less pronounced.

While previous research reported the successful deposition of anti-infective DNase coatings by long dipping times [34–37], our results indicate that AC-EPD could be a promising alternative to significantly reduce deposition times. In contrast, the use of dipping for fast DNase I deposition results in a reduced anti-infectivity and is only moderately effective towards *S. epidermidis* and not *P. aeruginosa*. Future research will be required to extensively compare short AC-EPD to long dipping as deposition strategy. Since

DNase-EPD outperforms the latter in terms of activity and shelf life at 4°C, additional studies should reveal whether this translates into an extended protection of the implant against biofilm formation in the body and/or a longer retention of anti-infectivity upon storage at 4°C. Specifically for the application as a coating on implants, DNases should not hamper tissue integration, i.e. adhesion and spreading of host cells on the implant. Previous *in vitro* studies of the adhesion and proliferation of different mammalian cell types on DNase coatings prepared by long dipping did not report any adverse effects [34–37]. In the future, this should be confirmed for DNase coatings prepared by short AC-EPD. To date, *in vivo* evaluation of DNase coatings has not been reported, yet it is essential to study the interplay with different host factors. The assessment in relevant pre-clinical models will be required in the future to estimate both the *in vivo* safety, as well as the *in vivo* efficacy to prevent biofilm formation.

5. Conclusions

In this study, AC-EPD was evaluated as a rapid deposition strategy to immobilize active DNase I coatings on PDA-functionalized Ti compared to the commonly applied diffusion methodology (i.e., classic dipping) for the same processing times. We observed that AC-EPD accelerates the protein immobilization and enables a thicker and more homogeneous film formation than dip-coating. A detailed investigation of the surface chemistry after each step in the deposition process by XPS and ToF-SIMS confirmed the presence of a DNase I monolayer on all DNase-treated samples after both coating methods. Yet, a selective deposition on electrodes which were coupled as anode during the high-amplitude half cycle was proven. PDA-related fragments were observed on the cathode (i.e. counter electrode), while a denser DNase I coating was found on the anode (i.e. working electrode). Furthermore, no signs of structural changes in the enzyme could be detected by ToF-SIMS for both deposition techniques. As such, a proof-of-concept for the AC-EPD application of enzymes on PDA-functionalized Ti surface was delivered.

Fresh AC-EPD-coated surfaces were approximately threefold more active than dip-coated surfaces. For both deposition strategies, the great majority of DNase was not permanently immobilized and released quickly from the surface, although coatings prepared with AC-EPD showed an additional slower sustained release of DNase activity. For both coating techniques, a small fraction of the activity was more stably retained to the surface, suggesting covalent coupling to the PDA functionalization layer. The differences in coating activity resulted into different *in vitro* anti-infective properties. While DNase-EPD significantly reduced biofilm formation of both *S. epidermidis* and *P. aeruginosa* over 20 h, DNase-dip only reduced *S. epidermidis* biofilms, albeit to a lesser extent. Overall, these results showed that 10 min AC-EPD, but not

10 min dipping, is a promising strategy for the fast immobilization of broad spectrum anti-infective DNase coatings on Ti.

6. Acknowledgements

This work was supported by the Research Foundation – Flanders (FWO) through a predoctoral grant to MVDG [1S43118N] and a grant for medium scale research infrastructure for the XPS VPIII [I006220N]; and by Internal Funds KU Leuven [C32/18/010, STG/17/024, AKUL/17/026]. The authors thank Dan Graham, Ph.D., for developing the NESAC/BIO Toolbox used in this study and NIH grant EB-002027 for supporting the toolbox development. We would like to also thank Dr. Joleen Masschelein at the Laboratory for Medicinal Chemistry at the Rega Institute (KU Leuven) for access to the CLARIOStar microplate reader. Furthermore, we are thankful for the support regarding ellipsometry (Prof. Rob Ameloot, Dr. Max Tietze) and AFM (Prof. Steven De Feyter) measurements.

7. References

[1] B.K.J. Bozic, S.M. Kurtz, E. Lau, K. Ong, T.P. Vail, D.J. Berry, The Epidemiology of Revision Total Hip Arthroplasty in the United States, J. Bone Jt. Surg. 91 (2009) 128–133. https://doi.org/10.2106/JBJS.H.00155.

[2] J.S. Van Epps, J.G. Younger, Implantable device-related infection, Shock. 46 (2016) 597–608. https://doi.org/10.1097/SHK.0000000000000692.

[3] X. Li, L. Sun, P. Zhang, Y. Wang, Novel approaches to combat medical device-associated biofilms, Coatings. 11 (2021) 1–31. https://doi.org/10.3390/coatings11030294.

[4] N. Reina, C. Delaunay, P. Chiron, N. Ramdane, M. Hamadouche, Infection as a cause of primary total hip arthroplasty revision and its predictive factors, Orthop. Traumatol. Surg. Res. 99 (2013) 555–561. https://doi.org/10.1016/j.otsr.2013.07.001.

[5] A. Postler, C. Lützner, F. Beyer, E. Tille, J. Lützner, Analysis of Total Knee Arthroplasty revision causes, BMC Musculoskelet. Disord. 19 (2018) 1–6. https://doi.org/10.1186/s12891-018-1977-y.

[6] M.A. Ritter, A. Farris, Outcome of infected total joint replacement., Orthopedics. 33 (2010). https://doi.org/http://dx.doi.org/10.3928/01477447-20100129-09.

[7] V. Boddapati, M.C. Fu, M.W. Tetreault, J.L. Blevins, S.S. Richardson, E.P. Su, Short-term

Complications After Revision Hip Arthroplasty for Prosthetic Joint Infection Are Increased Relative to Noninfectious Revisions, J. Arthroplasty. 33 (2018) 2997–3002. https://doi.org/10.1016/j.arth.2018.05.001.

[8] M. Haenle, C. Skripitz, W. Mittelmeier, R. Skripitz, Economic impact of infected total knee arthroplasty, Sci. World J. 2012 (2012). https://doi.org/10.1100/2012/196515.

[9] D. Hernández-Vaquero, M. Fernández-Fairen, A. Torres, A.M. Menzie, J.M. Fernández-Carreira, A. Murcia-Mazon, E. Guerado, L. Merzthal, Treatment of periprosthetic infections: An economic analysis, Sci. World J. 2013 (2013). https://doi.org/10.1155/2013/821650.

[10] S. Sivananthan, S. Goodman, M. Burke, Failure mechanisms in joint replacement, in: P.A. Revell (Ed.), Jt. Replace. Technol., 2nd ed., Elsevier, 2014: pp. 370–400. https://doi.org/10.1533/9780857098474.3.370.

[11] G. Garellick, J. Kärrholm, C. Rogmark, H. Peter, Swedish Hip Arthroplasty Register Annual Report 2019, 2019. https://doi.org/10.18158/H1BdmrOWu.

[12] S.M. Kurtz, E. Lau, H. Watson, J.K. Schmier, J. Parvizi, Economic burden of periprosthetic joint infection in the united states, J. Arthroplasty. 27 (2012) 61-65.e1. https://doi.org/10.1016/j.arth.2012.02.022.

[13] A.J. Tande, R. Patel, Prosthetic joint infection, Clin. Microbiol. Rev. 27 (2014) 302–345. https://doi.org/10.1128/CMR.00111-13.

[14] L. Drago, E. De Vecchi, F.-C.B.M. Wagenaar, D.F.M. Pakvis, L. Frommelt, J. Segreti, Diagnosis, in: K.-D. Kühn (Ed.), Manag. Periprosthetic Jt. Infect. A Glob. Perspect. Diagnosis, Treat. Options, Prev. Strateg. Their Econ. Impact, Springer-Verlag GmbH Germany, 2017: pp. 43–75. https://doi.org/10.1007/978-3-662-54469-3.

[15] M. Niinomi, C.J. Boehlert, Titanium alloys for biomedical applications, Springer Ser. Biomater. Sci. Eng. 3 (2015) 179–213. https://doi.org/10.1007/978-3-662-46836-4_8.

[16] C.R. Arciola, Y.H. An, D. Campoccia, M.E. Donati, L. Montanaro, Etiology of implant orthopedic infections: A survey on 1027 clinical isolates, Int. J. Artif. Organs. 28 (2005) 1091–1100. https://doi.org/10.1177/039139880502801106.

[17] L. Montanaro, P. Speziale, D. Campoccia, T. Ravaioli, I. Cangini, G. Pietrocola, S. Giannini, C.R. Arciola, Scenery of Staphylococcus implant infections in orthopedics, Future Microbiol. 6 (2011) 1329–1349. https://doi.org/10.2217/fmb.11.117.

[18] C.R. Arciola, D. Campoccia, L. Montanaro, Implant infections: Adhesion, biofilm formation and immune evasion, Nat. Rev. Microbiol. 16 (2018) 397–409. https://doi.org/10.1038/s41579-018-0019-y.

[19] M. Cerioli, C. Batailler, A. Conrad, S. Roux, T. Perpoint, A. Becker, C. Triffault-Fillit, S. Lustig, M.-H. Fessy, F. Laurent, F. Valour, C. Chidiac, T. Ferry, Pseudomonas aeruginosa Implant-Associated Bone and Joint Infections: Experience in a Regional Reference Center in France, Front. Med. 7 (2020) 1–7. https://doi.org/10.3389/fmed.2020.513242.

[20] M. Jacques, T.J. Marrie, J.W. Costerton, Review: Microbial colonization of prosthetic devices, Microb. Ecol. 13 (1987) 173–191. https://doi.org/10.1007/BF02024996.

[21] J.W. Costerton, Z. Lewandowski, D.E. Caldwell, D.R. Korber, H.M. Lapin-Scott, Microbial biofilms, Annu. Rev. Microbiol. 49 (1995) 711–745. https://doi.org/10.1201/9780203500224.

[22] H.C. Flemming, J. Wingender, The biofilm matrix, Nat. Rev. Microbiol. 8 (2010) 623–633. https://doi.org/10.1038/nrmicro2415.

[23] I.W. Sutherland, The biofilm matrix - An immobilized but dynamic microbial environment, Trends Microbiol. 9 (2001) 222–227. https://doi.org/10.1016/S0966-842X(01)02012-1.

[24] N. Høiby, T. Bjarnsholt, M. Givskov, S. Molin, O. Ciofu, Antibiotic resistance of bacterial biofilms, Int. J. Antimicrob. Agents. 35 (2010) 322–332. https://doi.org/10.1016/j.ijantimicag.2009.12.011.

[25] E. Roilides, M. Simitsopoulou, A. Katragkou, T.J. Walsh, How Biofilms Evade Host Defenses, Microbiol. Spectr. 3 (2015). https://doi.org/10.1128/microbiolspec.mb-0012-2014.

[26] E. Gómez-Barrena, J. Esteban, F. Medel, D. Molina-Manso, A. Ortiz-Pérez, J. Cordero-Ampuero, J.A. Puértolas, Bacterial adherence to separated modular components in joint prosthesis: A clinical study, J. Orthop. Res. 30 (2012) 1634–1639. https://doi.org/10.1002/jor.22114.

[27] H.O. Gbejuade, A.M. Lovering, J.C. Webb, The role of microbial biofilms in prosthetic joint infections: A review, Acta Orthop. 86 (2015) 147–158. https://doi.org/10.3109/17453674.2014.966290.

[28] A. Nana, S.B. Nelson, A. McLaren, A.F. Chen, What's new in musculoskeletal infection: Update on biofilms, J. Bone Jt. Surg. - Am. Vol. 98 (2016) 1226–1234.

https://doi.org/10.2106/JBJS.16.00300.

[29] M. Okshevsky, R.L. Meyer, The role of extracellular DNA in the establishment, maintenance and perpetuation of bacterial biofilms, Crit. Rev. Microbiol. 41 (2015) 341–352. https://doi.org/10.3109/1040841X.2013.841639.

[30] J.B. Kaplan, Therapeutic potential of biofilm-dispersing enzymes, 32 (2009) 545–554.

[31] M. Okshevsky, V.R. Regina, R.L. Meyer, Extracellular DNA as a target for biofilm control, Curr. Opin. Biotechnol. 33 (2015) 73–80. https://doi.org/10.1016/j.copbio.2014.12.002.

[32] C. Yang, M. Montgomery, Dornase alfa for cystic fibrosis, Cochrane Database Syst. Rev. (2018). https://doi.org/10.1002/14651858.CD001127.pub4.

[33] https://www.pulmozyme.com/patient/about-pulmozyme/how-it-works.html, How Pulmozyme works to fight cystic fibrosis (CF), Genet. (n.d.).

[34] J.J.T.M. Swartjes, T. Das, S. Sharifi, G. Subbiahdoss, P.K. Sharma, B.P. Krom, H.J. Busscher, H.C. Van Der Mei, A Functional DNase I Coating to Prevent Adhesion of Bacteria and the Formation of Biofi lm, 23 (2013) 2843–2849.

[35] S. Yuan, J. Zhao, S. Luan, S. Yan, W. Zheng, J. Yin, Nuclease-functionalized Poly(Styrene-b-isobutylene-b-styrene) surface with anti-infection and tissue integration bifunctions, Appl. Mater. Interfaces. 6 (2014) 18078–18086. https://doi.org/10.1021/am504955g.

[36] D. Alves, A. Magalhães, D. Grzywacz, D. Neubauer, W. Kamysz, M.O. Pereira, Co-immobilization of Palm and DNase I for the development of an effective anti-infective coating for catheter surfaces, Acta Biomater. 44 (2016) 313–322. https://doi.org/10.1016/j.actbio.2016.08.010.

[37] J. Ye, C. Shao, X. Zhang, X. Guo, P. Gao, Y. Cen, S. Ma, Y. Liu, Effects of DNase I coating of titanium on bacteria adhesion and biofilm formation, Mater. Sci. Eng. C. 78 (2017) 738–747. https://doi.org/10.1016/j.msec.2017.04.078.

[38] J.J.T.M. Swartjes, Innovative coatings for anti-bacterial surfaces, University of Groningen, 2015.

[39] A.R. Boccaccini, S. Keim, R. Ma, Y. Li, I. Zhitomirsky, Electrophoretic deposition of biomaterials, J. R. Soc. Interface. 7 (2010). https://doi.org/10.1098/rsif.2010.0156.focus.

[40] M. Ammam, Electrophoretic deposition under modulated electric fields: A review, RSC Adv. 2 (2012) 7633–7646. https://doi.org/10.1039/c2ra01342h.

[41] S. Seuss, A.R. Boccaccini, Electrophoretic deposition of biological macromolecules, drugs, and cells, Biomacromolecules. 14 (2013) 3355–3369. https://doi.org/10.1021/bm401021b.

[42] B. Neirinck, J. Fransaer, O. Van der Biest, J. Vleugels, Aqueous electrophoretic deposition in asymmetric AC electric fields (AC-EPD), Electrochem. Commun. 11 (2009) 57–60. https://doi.org/10.1016/j.elecom.2008.10.028.

[43] T. Yoshioka, A. Chávez-Valdez, J.A. Roether, D.W. Schubert, A.R. Boccaccini, AC electrophoretic deposition of organic-inorganic composite coatings, J. Colloid Interface Sci. 392 (2013) 167–171. https://doi.org/10.1016/j.jcis.2012.09.087.

[44] A. Chávez-Valdez, A.R. Boccaccini, Innovations in electrophoretic deposition: Alternating current and pulsed direct current methods, Electrochim. Acta. 65 (2012) 70–89. https://doi.org/10.1016/j.electacta.2012.01.015.

[45] B. Neirinck, L. Van Mellaert, J. Fransaer, O. Van der Biest, J. Anné, J. Vleugels, Electrophoretic deposition of bacterial cells, Electrochem. Commun. 11 (2009) 1842–1845. https://doi.org/10.1016/j.elecom.2009.07.033.

[46] M. Ammam, J. Fransaer, AC-electrophoretic deposition of glucose oxidase, Biosens. Bioelectron. 25 (2009) 191–197. https://doi.org/10.1016/j.bios.2009.06.036.

[47] A. Braem, K. De Brucker, N. Delattin, M.S. Killian, M.B.J. Roeffaers, T. Yoshioka, S. Hayakawa, P. Schmuki, B.P.A. Cammue, S. Virtanen, K. Thevissen, B. Neirinck, Alternating Current Electrophoretic Deposition for the Immobilization of Antimicrobial Agents on Titanium Implant Surfaces, ACS Appl. Mater. Interfaces. 9 (2017) 8533–8546. https://doi.org/10.1021/acsami.6b16433.

[48] I. Horcas, R. Fernández, J.M. Gómez-Rodríguez, J. Colchero, J. Gómez-Herrero, A.M. Baro, WSXM: A software for scanning probe microscopy and a tool for nanotechnology, Rev. Sci. Instrum. 78 (2007) 013705-1–8. https://doi.org/10.1063/1.2432410.

[49] J.A. De Feijter, J. Benjamins, F.A. Veer, Ellipsometry as a tool to study the adsorption behavior of synthetic and biopolymers at the air–water interface, Biopolymers. 17 (1978) 1759–1772. https://doi.org/doi:10.1002/bip.1978.360170711.

[50] T. Berlind, P. Tengvall, L. Hultman, H. Arwin, Protein adsorption on thin films of carbon and carbon nitride monitored with in situ ellipsometry, Acta Biomater. 7 (2011) 1369–1378. https://doi.org/10.1016/j.actbio.2010.10.024.

[51] D.K. Owens, Estimation of the Surface Free Energy of Polymers, J. Appl. Polym. Sci. 13

(1969) 1741–1747.

[52] C.J. van Oss, M.K. Chaudhury, R.J. Good, Monopolar surfaces, Adv. Colloid Interface Sci. 28 (1987) 35–64.

[53] C.J. Van Oss, R.J. Good, M.K. Chaudhury, Additive and nonadditive surface tension components and the interpretation of contact angles, Langmuir. 4 (2002) 884–891. https://doi.org/10.1021/la00082a018.

[54] http://www.nb.uw.edu/mvsa/multivariate-surface-analysis-homepage, (n.d.).

[55] M.S. Killian, A.J. Taylor, D.G. Castner, Stabilization of dry protein coatings with compatible solutes, Biointerphases. 13 (2018) 06E401-8. https://doi.org/10.1116/1.5031189.

[56] and J.S.-V. D. L. Massart, B. G. M. Vandeginste, L. M. C. Buydens, S. De Jong, P. J. Lewi, Handbook of Chemometrics and Qualimetrics: Part B, 1998. http://dblp.uni-trier.de/db/journals/jcisd/jcisd38.html#Slutsky98a.

[57] M. Van der Gucht, M.K. Aktan, H. Hendrix, G. Vande Velde, J. Paeshuyse, A. Braem, R. Lavigne, qDNase assay: A quantitative method for real-time assessment of DNase activity on coated surfaces, Biochem. Biophys. Res. Commun. (2020). https://doi.org/10.1016/j.bbrc.2020.10.050.

[58] S. Delgado, R. Arroyo, E. Jiménez, M.L. Marín, R. Del Campo, L. Fernández, J.M. Rodríguez, Staphylococcus epidermidis strains isolated from breast milk of women suffering infectious mastitis: Potential virulence traits and resistance to antibiotics, BMC Microbiol. 9 (2009). https://doi.org/10.1186/1471-2180-9-82.

[59] J. Schindelin, I. Arganda-Carreras, E. Frise, V. Kaynig, M. Longair, T. Pietzsch, S. Preibisch, C. Rueden, S. Saalfeld, B. Schmid, J.Y. Tinevez, D.J. White, V. Hartenstein, K. Eliceiri, P. Tomancak, A. Cardona, Fiji: An open-source platform for biological-image analysis, Nat. Methods. 9 (2012) 676–682. https://doi.org/10.1038/nmeth.2019.

[60] C.A. Schneider, W.S. Rasband, K.W. Eliceiri, NIH Image to ImageJ: 25 years of image analysis, Nat. Methods. 9 (2012) 671–675. https://doi.org/10.1038/nmeth.2089.

[61] A. Heydorn, A.T. Nielsen, M. Hentzer, C. Sternberg, M. Givskov, B.K. Ersbøll, S. Molin, Quantification of biofilm structures by the novel computer program COMSTAT., Microbiol. 146 (2000) 2395–2407. https://doi.org/10.1099/00221287-146-10-2395.

[62] M. Vorregaard, Comstat2 - a modern 3D image analysis environment for biofilms, in

Informatics and Mathematical Modelling, Technical University of Denmark: Kongens Lyngby, Denmark, 2008.

[63] Comstat2, (2008).

[64] H.S. Kim, T.-H. Liao, Isoelectric focusing of multiple forms of DNase in thin layers of polyacrylamide gel and detection of enzymatic activity with a zymogrm method following separation.pdf, Anal. Biochem. 119 (1982) 96–101.

[65] Y.H. Ding, M. Floren, W. Tan, Mussel-inspired polydopamine for bio-surface functionalization, 2 (2016) 121–136.

[66] C.Y. Chien, T.Y. Liu, W.H. Kuo, M.J. Wang, W.B. Tsai, Dopamine-assisted immobilization of hydroxyapatite nanoparticles and RGD peptides to improve the osteoconductivity of titanium, J. Biomed. Mater. Res. - Part A. 101 A (2013) 740–747. https://doi.org/10.1002/jbm.a.34376.

[67] F. Bernsmann, B. Frisch, C. Ringwald, V. Ball, Protein adsorption on dopamine-melanin films: Role of electrostatic interactions inferred from ζ-potential measurements versus chemisorption, J. Colloid Interface Sci. 344 (2010) 54–60. https://doi.org/10.1016/j.jcis.2009.12.052.

[68] M.M. Shirolkar, D. Phase, V. Sathe, J. Rodrguez-Carvajal, R.J. Choudhary, S.K. Kulkarni, Relation between crystallinity and chemical nature of surface on wettability: A study on pulsed laser deposited TiO2 thin films, J. Appl. Phys. 109 (2011) 123512-1-123512–10. https://doi.org/10.1063/1.3594695.

[69] C. Sittig, M. Textor, N.D. Spencer, M. Wieland, P.H. Vallotton, Surface characterization of implant materials c.p. Ti, Ti-6Al-7Nb and Ti-6Al-4V with different pretreatments, J. Mater. Sci. Mater. Med. 10 (1999) 35–46. https://doi.org/10.1023/A:1008840026907.

[70] E. Vanderleyden, S. Van Bael, Y.C. Chai, J.P. Kruth, J. Schrooten, P. Dubruel, Gelatin functionalised porous titanium alloy implants for orthopaedic applications, Mater. Sci. Eng. C. 42 (2014) 396–404. https://doi.org/10.1016/j.msec.2014.05.048.

[71] S.T. Abrahami, T. Hauffman, J.M.M. De Kok, J.M.C. Mol, H. Terryn, XPS Analysis of the Surface Chemistry and Interfacial Bonding of Barrier-Type Cr(VI)-Free Anodic Oxides, J. Phys. Chem. C. 119 (2015) 19967–19975. https://doi.org/10.1021/acs.jpcc.5b05958.

[72] M. Pisarek, A. Roguska, M. Andrzejczuk, L. Marcon, S. Szunerits, M. Lewandowska, M. Janik-Czachor, Effect of two-step functionalization of Ti by chemical processes on protein

adsorption, Appl. Surf. Sci. 257 (2011) 8196–8204. https://doi.org/10.1016/j.apsusc.2011.03.120.

[73] J.S. Stevens, A.C. De Luca, M. Pelendritis, G. Terenghi, S. Downes, S.L.M. Schroeder, Quantitative analysis of complex amino acids and RGD peptides by X-ray photoelectron spectroscopy (XPS), Surf. Interface Anal. 45 (2013) 1238–1246. https://doi.org/10.1002/sia.5261.

[74] R.A. Zangmeister, T.A. Morris, M.J. Tarlov, Characterization of polydopamine thin films deposited at short times by autoxidation of dopamine, Langmuir. 29 (2013) 8619–8628. https://doi.org/10.1021/la400587j.

[75] M.S. Killian, H.M. Krebs, P. Schmuki, Protein denaturation detected by time-of-flight secondary ion mass spectrometry, Langmuir. 27 (2011) 7510–7515. https://doi.org/10.1021/la200704s.

[76] L. Besra, M. Liu, A review on fundamentals and applications of electrophoretic deposition (EPD), Prog. Mater. Sci. 52 (2007) 1–61. https://doi.org/10.1016/j.pmatsci.2006.07.001.

[77] L. Lauková, B. Konečná, L. Janovičová, B. Vlková, P. Celec, Deoxyribonucleases and their applications in biomedicine, Biomolecules. 10 (2020) 1–20. https://doi.org/10.3390/biom10071036.

[78] M. Ammam, J. Fransaer, Effects of AC-Electrolysis on the Enzymatic Activity of Glucose Oxidase, Electroanalysis. 23 (2011) 755–763. https://doi.org/10.1002/elan.201000598.

[79] L. Le Guéhennec, A. Soueidan, P. Layrolle, Y. Amouriq, Surface treatments of titanium dental implants for rapid osseointegration, Dent. Mater. 23 (2007) 844–854. https://doi.org/10.1016/j.dental.2006.06.025.

[80] J. Park, S. Bauer, A. Pittrof, M.S. Killian, P. Schmuki, K. Von Der Mark, Synergistic control of mesenchymal stem cell differentiation by nanoscale surface geometry and immobilized growth factors on TiO2 nanotubes, Small. 8 (2012) 98–107. https://doi.org/10.1002/smll.201100790.

[81] J. Barberi, S. Spriano, Titanium and protein adsorption: An overview of mechanisms and effects of surface features, Materials (Basel). 14 (2021) 1–41. https://doi.org/10.3390/ma14071590.

[82] J. Veerasamy, S. Ramamoorthi, M. Vijayasarathy, P. Anandagopu, E. Rajasekaran, Role of large hydrophobic residues in proteins, Bioinformation. 9 (2009) 409–412.

[83] K.D. Saint Jean, K.D. Henderson, C.L. Chrom, L.E. Abiuso, L.M. Renn, G.A. Caputo, Effects of Hydrophobic Amino Acid Substitutions on Antimicrobial Peptide Behavior, Probiotics Antimicrob. Proteins. 10 (2018) 408–419. https://doi.org/10.1007/s12602-017-9345-z.

[84] C. Zhang, L. Gong, L. Xiang, Y. Du, W. Hu, H. Zeng, Z. Xu, Deposition and Adhesion of Polydopamine on the Surfaces of Varying Wettability, ACS Appl. Mater. Interfaces. 9 (2017) 30943–30950. https://doi.org/10.1021/acsami.7b09774.

[85] V. Ball, D. Del Frari, V. Toniazzo, D. Ruch, Kinetics of polydopamine film deposition as a function of pH and dopamine concentration: Insights in the polydopamine deposition mechanism, J. Colloid Interface Sci. 386 (2012) 366–372. https://doi.org/10.1016/j.jcis.2012.07.030.

[86] B. Lizarraga, D. Sanchez-Romero, A. Gil, E. Melgar, The role of Ca2+ on pH-induced hydrodynamic changes of bovine pancreatic deoxyribonuclease A, J. Biol. Chem. 253 (1978) 3191–3195. https://doi.org/10.1016/S0021-9258(17)40822-2.

[87] Z. Qin, Y. Ou, L. Yang, Y. Zhu, Role of autolysin-mediated DNA release in biofilm formation of Staphylococcus epidermidis, Microbiol. 153 (2007) 2083–2092. https://doi.org/10.1099/mic.0.2007/006031-0.

[88] S.R. Hymes, T.M. Randis, T.Y. Sun, A.J. Ratner, DNase Inhibits Gardnerella vaginalis Biofilms In Vitro and In Vivo, J. Infect. Dis. 207 (2013) 1491–1497. https://doi.org/10.1093/infdis/jit047.

[89] S. Schlafer, J. Garcia, R.L. Meyer, M. Vaeth, K.W. Neuhaus, Effect of DNase treatment on adhesion and early biofilm formation of Enterococcus faecalis, Eur. Endod. J. 3 (2018) 82–86. https://doi.org/10.14744/eej.2018.55264.

[90] K. Nakanishi, T. Sakiyama, K. Imamura, On the Adsorption of Proteins on Solid Surfaces , a Common but Very Complicated Phenomenon, 91 (2001) 233–244.

[91] A. Gristina, The Classic: Biomaterial-Centered Infection: Microbial Adhesion versus Tissue Integration, Clin. Orthop. Relat. Res. 427 (2004) 4–12. https://doi.org/10.1097/01.blo.0000145156.89115.12.

[92] S.M. Shiels, L.H. Mangum, J.C. Wenke, Revisiting the “race for the surface” in a pre-clinical model of implant infection, Eur. Cells Mater. 39 (2020) 77–95. https://doi.org/10.22203/eCM.v039a05.

[93] K. Nemoto, K. Hirota, K. Murakami, K. Taniguti, H. Murata, D. Viducic, Y. Miyake, Effect of Varidase (Streptodornase) on Biofilm Formed by Pseudomonas aeruginosa, Chemotherapy. 49 (2003) 121–125. https://doi.org/10.1159/000070617.

[94] D. Gutiérrez, Y. Briers, L. Rodríguez-Rubio, B. Martínez, A. Rodríguez, R. Lavigne, P. García, Role of the Pre-neck Appendage Protein (Dpo7) from Phage vB _ SepiS-phiIPLA7 as an Anti-biofilm Agent in Staphylococcal Species, Front. Microbiol. 6 (2015) 1–10. https://doi.org/10.3389/fmicb.2015.01315.